
MORB-derived amphibolites in the Paleozoic basement of the Aluminé Igneous-Metamorphic Complex, Neuquén, Argentina: Decoding its genesis, P-T evolution and pre-Andean regional correlations

I. URRAZA¹ S. DELPINO² L. GRECCO¹

¹Departamento de Geología, Universidad Nacional del Sur

San Juan 670, Bahía Blanca, Argentina. Urraza E-mail: iurraza@uns.edu.ar

Tel: +54(0291) 4595101

² INGEOSUR (CONICET-UNS)

Alem 1253, Cuerpo B 1 piso. Oficina 110, Bahía Blanca, Argentina. Tel: +54 (0291) 4595101 interno 3033.

| A B S T R A C T |

Amphibolites included in the metapelitic sequence and as xenoliths in intrusive magmatic rocks outcropping in the southern sector of the Aluminé Igneous-Metamorphic Complex (AIMC), Neuquén, Argentina, are studied in detail in order to determine their origin and their subsequent metamorphic evolution. Field evidence and whole-rock geochemistry indicate that these rocks were derived from a Mid-Ocean Ridge Basalt (MORB)-type protolith, and were accreted as tectonic slices into the metapelitic sequence that mainly formed the basal accretionary prism associated with a pre-Andean SW-NE subduction setting. Phase relationships, geochemistry of mineral assemblages and geothermobarometry indicate the presence of at least two metamorphic events (M_1 1.9–3.9kbar, 677–745°C and M_2 6.4kbar, 723°C) framed in a counterclockwise P-T path, comparable to those previously determined for the metapelitic country-rocks and metatroctolites outcropping in the same sector of the AIMC. Based on regional correlations and the agreement in the petrological, geochemical, geochronological and structural characteristics, we suggest that the MORB-derived Ñorquinco amphibolites and neighboring aluminous metasedimentary basement rocks of the AIMC belong to the eastern prolongation of the Western Series of the Coastal Accretionary Complex of Central Chile in west-central Argentina territory.

KEYWORDS MORB. Amphibolites. Thermobarometry. P-T path. Late Paleozoic. Triassic. Accretionary prism.

INTRODUCTION

The evolution of the Gondwana margin after the Famatinian Orogeny is registered in metamorphic complexes of the Argentinian and Chilean territories (18°S-54°S). Several bodies of amphibolites occur along the accretionary

complexes related to subduction in southwestern margin of Gondwana during Middle Paleozoic times. The origin and tectono-metamorphic evolution of amphibolites have high petrological interest, since most of them are derived from igneous protoliths (Leake, 1964). In addition, amphibolites have proven to be of relevant importance in determining

the thermal evolution of many metamorphic complexes related to subduction, such as the Punta Choros (Creixell *et al.*, 2012), Las Tortolas Formation (Fuentes *et al.*, 2018) and Choapa Metamorphic Complex in northern Chile; Pichulemu and Constitución region (Hyppolito *et al.*, 2014; Willner, 2005), Los Pabilos (Kato *et al.* 2009; Willner *et al.*, 2004b, 2011), Bahía Mansa (Duhart 2001, among others) in Central Coastal cordillera and Diego de Almagro metamorphic Complex (Angiboust *et al.*, 2017; Hyppolito *et al.*, 2016; Willner *et al.*, 2004a) in southern Chile.

The studied rocks in this contribution are also included in a metamorphic complex developed in the Gondwana margin in Argentinean territory defined as Aluminé Igneous and Metamorphic Complex (AIMC) (Urraza *et al.*, 2011; Urraza, 2014), located in central-West Neuquén Province (39°S). The geology of AIMC preserves several characteristics that allow linking it with Chilean metamorphic complexes. In the southern portion of central Chile (39°S) amphibolites have been deeply studied not only by the presence of massive sulphide deposits recorded in metabasic rocks, but also because these rocks are chemically comparable to mid-ocean ridge basalts (Hervé, 1988 and references therein), suggesting the existence of a broad pre-Carboniferous oceanic basin to the south.

Although the P-T evolution of metamorphic complexes that preserves amphibolites has been deeply studied in Chile, in Argentina there have been no detailed studies of the evolution of the amphibolitic rocks outcropping at the same latitude. Taking this into account, special attention has been placed on amphibolite bodies to establish lithological, geochemical and evolutionary relationships between both regions, where ocean crust derived rocks preserve different P-T evolutions (*e.g.* in Pichilemu-Constitución 35°–37°S, peak P-T conditions of 7.0–9.3kbar, 380–420°C, Bahía Mansa metamorphic complex, Los Pabilos block 41°S with P-T conditions of 600–760°C, 11–16.5kbar for stage I and 350–500°C, 10–14kbar for stage II).

The main goal of this contribution is to establish the genesis and P-T path followed by the amphibolites of the AIMC, and to correlate the results with those obtained in the metapelitic country-rocks (Urraza *et al.*, 2009) and troctolitic metagabbros (Urraza *et al.*, 2015). AIMC rocks are considered part of an accretionary prism developed along the southwestern margin of Gondwana during Middle Paleozoic times (Urraza, 2014). In this regard, a second aim derived from the results of the present and previous studies is to propose regional correlations between the AIMC of center-West Argentina and the metamorphic complexes developed along the Coastal Cordillera in the Chilean territory.

GEOLOGICAL SETTING

Paleozoic tectonic evolution of southwestern Gondwana margin

The AIMC forms part of the proto-Andean margin of Gondwana, which records a long history of terrane accretion during the Paleozoic (Martinez *et al.*, 2011; Pankhurst *et al.*, 2003; Ramos, 2004). The continental growth along the western margin of South America started after the amalgamation of western Gondwana during the Brasiliano-Pan-African orogeny (Pankhurst *et al.*, 1998). At 570–520Ma the siliciclastic sediments deposited in a passive margin were accreted and partly incorporated into a magmatic arc (Pampean Mobile Belt, Rapela, 2000; Willner *et al.*, 2004b). At 490–420Ma an extensive magmatic arc associated with the development of medium to high-grade metamorphic rocks, formed in the western and central part of the Eastern Sierras Pampeanas (Famatinian Mobile Belt; Rapela, 2000). The allochthonous Cuyania Terrane exposed in the Argentinian Precordillera was accreted to South America at 29°–36°S between 460–435Ma (*e.g.* Casquet *et al.*, 2001; Castro de Machuca *et al.*, 2012; Ramos, 2000). The Cordillera Frontal basement assigned to the Chilenia terrane by Ramos *et al.* (1984) docked to western Gondwana during Late Devonian times. Ramos *et al.* (1986) proposed a separate “Chilenia” terrane mostly based on the presence of strongly metamorphosed-retrogressed ultrabasic bodies within a metamorphic belt in the Frontal Cordillera and western Precordillera of Argentina. Heredia *et al.* (2018), showed that the Chi-Cu (Chilenia-Cuyania) continental fragment (Cuyo Sector) is an allochthonous fragment, a terrane with a peri-Laurentic origin. Willner *et al.* (2011) proposed that the Chilenia terrane is bounded by two contrasting metamorphic belts with high-pressure rocks (Fig. 1A): i) the Guarguaraz Metamorphic Complex at the suture between Cuyania and Chilenia in western Argentina (longitude 69°W), which has characteristics of a Paleozoic collision zone (Massonne and Calderón, 2008; Willner *et al.*, 2008) and ii) the basement of the Coastal Cordillera in central Chile (longitude 72°W), representing a Late Paleozoic coastal accretionary prism (*e.g.* Glodny *et al.*, 2005; Hervé, 1988; Hyppolito *et al.*, 2014; Richter *et al.*, 2007; Willner, 2005; Willner *et al.*, 2005). In the Chilean Coastal Cordillera, two units, the Western and Eastern Series, constitute coeval parts of a Late Palaeozoic paired metamorphic belt dominated by siliciclastic metasediments. The western series also contain rocks from the upper oceanic crust (up to 10–15% intercalation interpreted as disrupted oceanic crust) accreted upon frontal and basal accretion. These accretionary and collisional orogens have been extensively studied and discussed since they have played a significant role in the evolution of the western margin of South America (Vaughan and Pankhurst, 2008).

Particularly, the AIMC sector between 38° and 40°S and 71° and 71°25'W shows a high complexity, which probably derives from its location in the transition between Chilenia and Cuyania terranes to the North, and the North-Patagonian Massif to the South (Fig. 1, modified after Vaughan and Pankhurst, 2008). Although this region constitutes a key area for understanding the evolution of the proto-Andean margin, detailed studies focused on its basement are still scarce (e.g. García-Sansegundo et al., 2009; Martínez Dopico et al., 2011; Martínez et al., 2011).

Geology of southern Aluminé Igneous-Metamorphic Complex (AIMC)

The AIMC, located between 38°30'–39°15'S and 71°–71°25'W, consists of Paleozoic igneous and metamorphic rocks (360–260Ma) intruded by Cretaceous rocks of the Patagonian Batholith (PB) (Urraza et al., 2008a, 2009,

2011, 2014). The basement of the AIMC is mainly constituted by a medium-high grade metasedimentary sequence composed of andalusite micaschists, garnet-biotite paragneisses and migmatites. Amphibolites occur as elongated lenses concordant with the tectonic structure of the para-derived rocks. Basement rocks of the AIMC were intruded by late ~300Ma diorites, tonalites, and gabbros. The late Paleozoic metasedimentary and metaigneous rocks began to be intruded by the igneous bodies at the onset of the Andean subduction, at ca. 150Ma in this latitude (Hervé et al., 2007).

The studied area is limited by the Pino Hachado–Picún Leufú (PH-PL) and the Nahuel Huapi (NH) megalineaments, defined by Ramos (1978), as the Aluminé Batholithic Belt. This area belongs to the northern part of the Patagonian Batholith in Neuquén Cordillera. The AIMC (Fig. 1B) is defined in Urraza et al. (2011) as basement conformed by

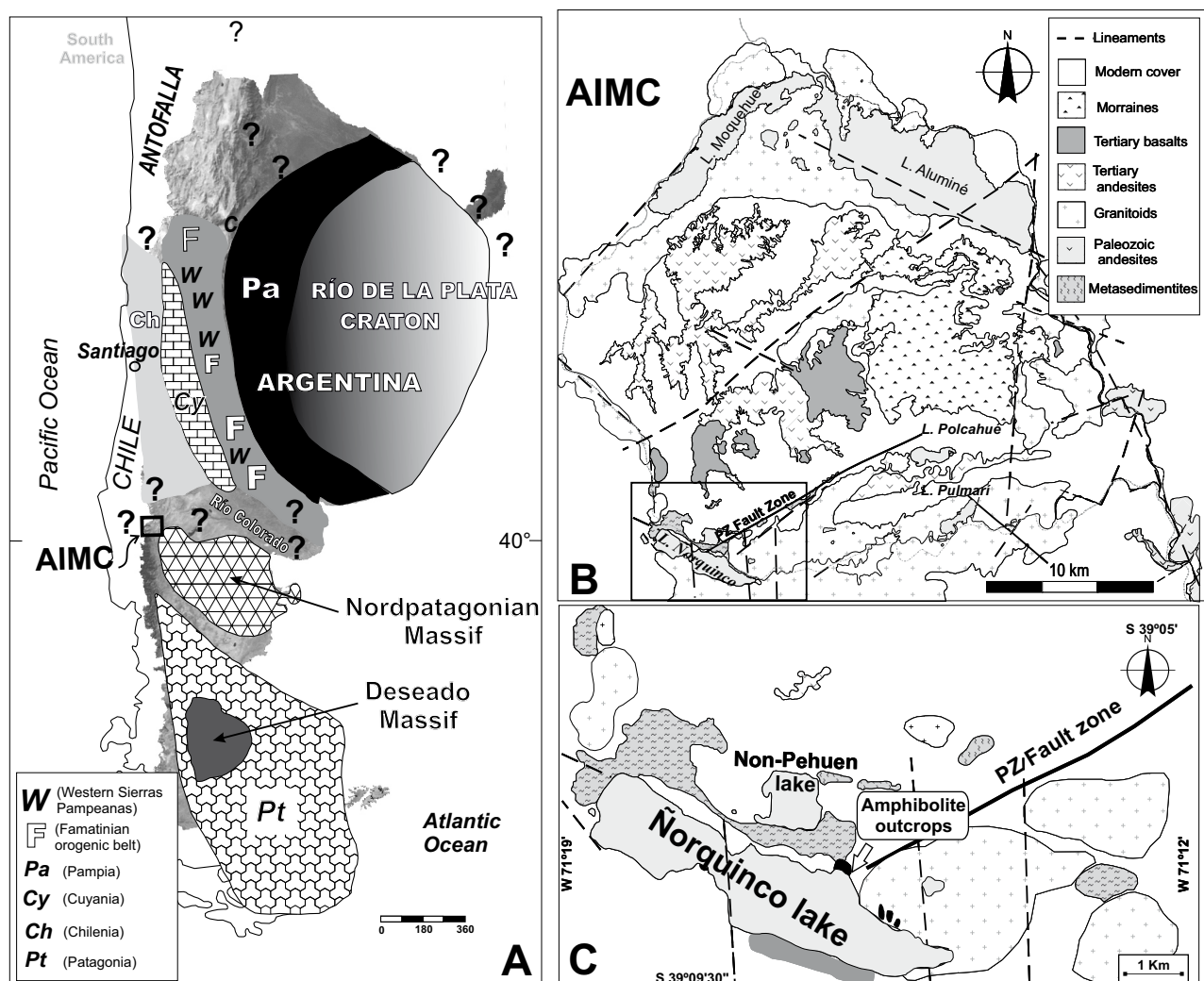


FIGURE 1. A) Location of AIMC in the Argentinean geological context (modified from Vaughan and Pankhurst, 2008). Question marks correspond to scarcely studied or undefined geological areas. B) Geological map of the AIMC showing the location of the Norquínco lake studied area. C) Simplified geological map of the Norquínco metamorphic and igneous rocks, pointing out the studied amphibolite outcrops.

pre-Andean metasedimentary and metaigneous rocks and andean intrusive igneous bodies, outcropping in the area located between the Aluminé, Moquehue, Ñorquinco and Pulmarí lakes in the Neuquén province, Argentina.

The Ñorquinco area is located in the southern sector of the AIMC (39°07'S–71°15'W) and consists of schists, gneisses and amphibolites, intruded by 309±11Ma troctolitic metagabbros and metatonalites and Mesozoic granodiorites (Urraza *et al.*, 2011, 2014) (Fig. 1C). The metamorphic series of AIMC contain strongly foliated gneisses and amphibolites, both affected by two metamorphic-deformational events: i) the first one developed under low pressure amphibolite facies conditions (up to 620°C and 3.8kbar) and ii) a mylonitic event developed under medium-pressure amphibolite facies conditions, in the range 6.2–6.7kbar and 605–620°C. The first metamorphic event was dated using monazite U-Th-Pb geochronology from a schist sample, which yielded a metamorphic age of ~360Ma. (Urraza *et al.*, 2008b). Martínez Dopico (2008) defined three metamorphic events for the amphibolites of the Ñorquinco area: i) the first event occurred under greenschist facies conditions at 550°C and 4.7kbar ii) a second greenschist facies conditions event produced at 450°C and 2.3kbar and iii) a third event that took place under prehnite-pumpellyite facies conditions at 300°C and 2.4kbar.

FIELD DESCRIPTION AND PETROGRAPHY OF 'IN SITU' AMPHIBOLITES, AMPHIBOLITE-XENOLITHS AND GRANODIORITES WITH XENOLITHS

The studied *in situ* amphibolites are interlayered with the metasedimentary sequences (Fig. 2A, B), but amphibolites also occur as amphibolitic xenoliths included in igneous plutonic rocks (see below and Figs. 3.1, 3.2). However, in the Puesto Zapata – Arroyo Relem area (2km to the northeast from Ñorquinco area) amphibolites appear only as xenoliths included in igneous rocks (Fig. 3C, D, E). Description of both occurrences is given below:

In situ amphibolites

At the Ñorquinco lake amphibolites occur as thin foliated bands mainly composed of plagioclase and amphibole. These rocks show “lit par lit” granitic material injected along the foliation planes (Fig. 2A, C). Both, compositional foliation and injected concordant veins, are asymmetrically folded (Fig. 2A). An increase of mineral grain size, reaching up to 1mm, is observed along the fold hinges (Fig. 2C). Irregular granitic veins few mm to 3cm in thickness, cross cut both foliations and thin concordant injections (Fig. 2A, D). A second foliation with injection of granitic material was also developed in a centimeter to meter scale fold hinge observed in an amphibolite outcrop (Fig.

2B). This foliation appears to be an axial plane foliation which roughly coincides in orientation with thicker granitic veins cutting first foliation and “lit par lit” injections at low angle in the fold limbs (Fig. 2A).

Under the microscope, amphibolites mainly consist of light to dark green pleochroic amphibole (55-60%, up to 250µm size), plagioclase (25-30%, 100-300µm), interstitial quartz (5-10%), opaque minerals (5%) and very scarce biotite partially replacing amphibole and ilmenite (Fig. 2D, E). Foliation is mainly defined by the preferential orientation of amphibole forming a nematoblastic texture. Foliation is also enhanced by the alternation of melanocratic (amphibolitic) and leucocratic (quartzo-feldspathic “lit par lit” injections) layers (Fig. 2C).

Plagioclase shows recrystallization forming polygonal grains of up to 500µm distributed in the matrix, and up to 1000µm in discordant irregular veins. Small relicts of Fe-Mg amphibole are recognizable with the help of the electron microscope (Fig. 2F). Abundant apatite is present as accessory mineral.

Amphibolite xenoliths

Amphibolites are found as xenoliths in granodiorites and tonalites of the Ñorquinco zone (Fig. 3A, B) and in the Arroyo Relem area (Fig. 3C, D). In Puesto Zapata and Arroyo Relem areas, granodiorites contain amphibolite xenoliths with different sizes and shapes, from small fragments with rounded or irregular contacts to large blocks of a few meters in size. The tonalites and granodiorites of the Ñorquinco area present not only amphibolite xenoliths, but also metapelite xenoliths. Amphibolite xenoliths show a granoblastic texture and are composed of $Qz+Pl+Kfs+Bt±Fe-Mg-Amp+Ca-Amp+Opq$ (abbreviations after Whitney and Evans, 2010). Quartz is present as recrystallized aggregates with 120° triple junctions and up to 1mm in mineral grain size. Pleochroic dark brown to reddish brown biotite, shows some flexures in the cleavage planes and partially replaces both types of amphiboles. Plagioclase develops bulging of up to 500µm along grain boundaries and recrystallized grains of equivalent sizes (400-600µm) forming 120° triple junctions. Two types of amphiboles were recognized: a high-birefringence pale-green amphibole, which is replaced by a low-birefringence dark-green amphibole. The amphibolite xenoliths preserve comparable texture and mineralogy to the *in situ* amphibolite outcrops described in Figure 2, except for the presence of K-feldspar and greater modal amounts of quartz and biotite, possible due to interaction with the host rocks.

Igneous host rocks

Amphibolitic xenoliths (sample AXG: Amphibolitic Xenoliths Granodiorites) are spatially associated with

sectors where *in situ* amphibolites occur. Thus, the lack of mafic inclusions in some of the intrusive bodies (e.g. southern sector of the AIMC, sample FAXG (Free Amphibolites Xenoliths Granodiorites) is attributed to the absence or scarcity of amphibolites in their emplacement host-rocks. The granodiorites and tonalite rocks are dark to pale grey, medium to coarse-grained and have subhedral to anhedral granular texture (Fig. 4A, B). The main minerals are plagioclase (45–40% modal), K-feldspar (2–15%), hornblende (10–20%), biotite (10–15%) and quartz (14–

20%). Common accessory minerals are zircon, titanite, apatite and magnetite and secondary minerals are chlorite, sericite and epidote. Plagioclase (oligoclase-andesine) forms euhedral to subhedral tabular crystals of 1.7mm to 5cm in length. It is locally zoned and twinned; other grains show subgrains and deformation twins. K-feldspar locally shows graphic texture, others appear interstitial among plagioclase, hornblende and biotite. Quartz forms 0.5–2.0mm recrystallized grains showing triple junctions. Hornblende is euhedral to subhedral (2–8mm in length).

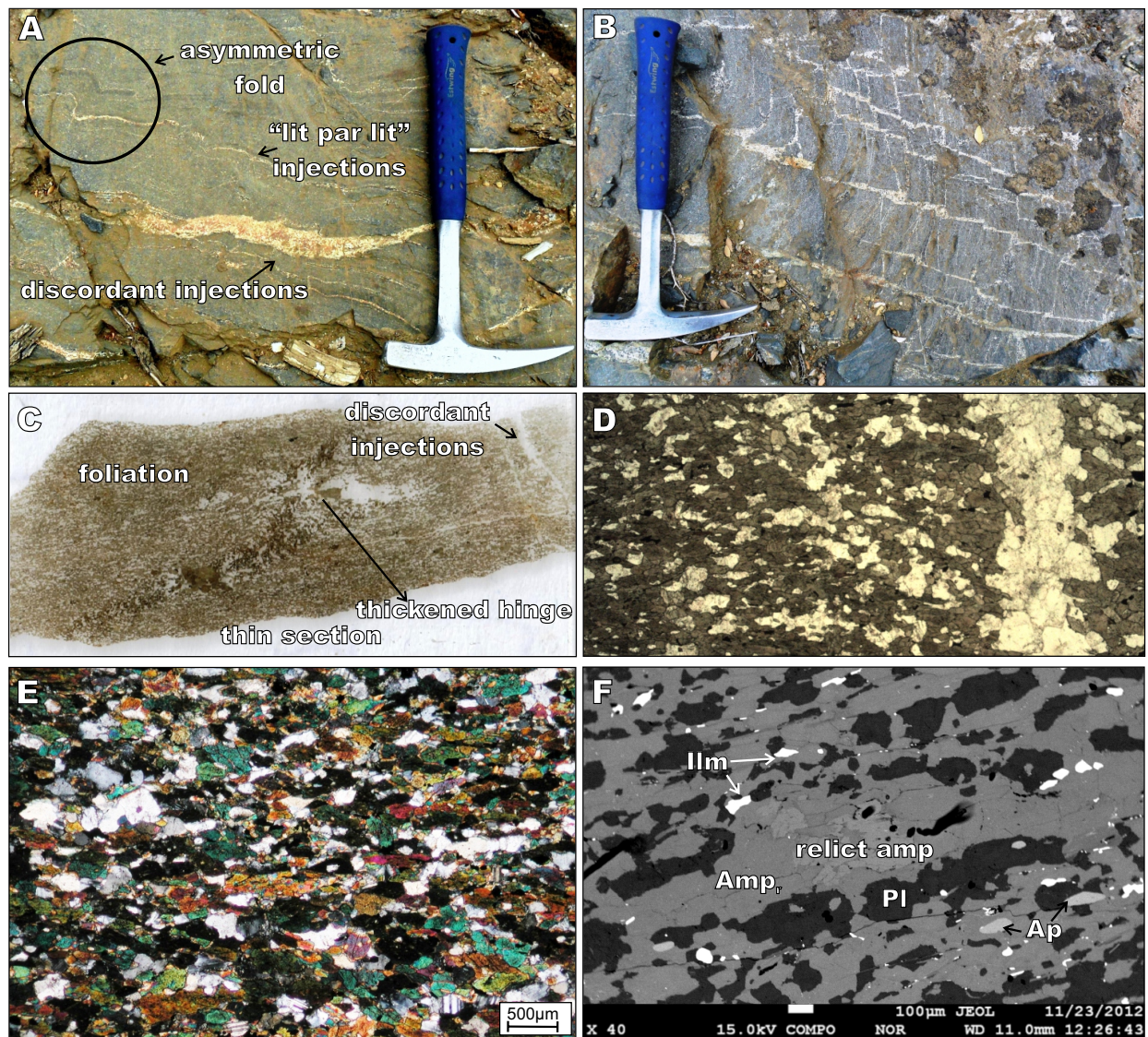


FIGURE 2. Ñorquinco lake amphibolites. A) Mesoscopic view of “lit par lit” granitic injections concordant with first foliation, cut by discordant granitic injections of variable sizes and shapes. Note asymmetric folding affecting a first foliation and “lit par lit” concordant injections. B) Fold hinge observed in an amphibolite outcrop. Note folded early foliation and “lit par lit” injections, cut at a high angle by a second foliation also filled with granitic material. C) Scanned amphibolite thin section showing nematoblastic texture and asymmetric folding affecting the early foliation. Note “lit par lit” thin concordant injections and development of coarser grain size in the fold hinges. D) Thin section showing green amphibole and plagioclase arranged in a nematoblastic texture. Scarce quartz and opaques are also present. Note to the right a coarser grained granitic vein with very irregular borders, cutting the early foliation at a very high-angle (plane polarized light). E) Idem D, with crossed nicols. F) Back-scattered electrons image showing very irregular relict Fe-Mg-amphibole (light grey), porphyroblasts and recrystallized Ca-amphibole (medium grey), recrystallized plagioclase (dark grey) and accessory minerals ilmenite (white) and apatite (pearl grey). Abbreviations after Whitney and Evans (2010).

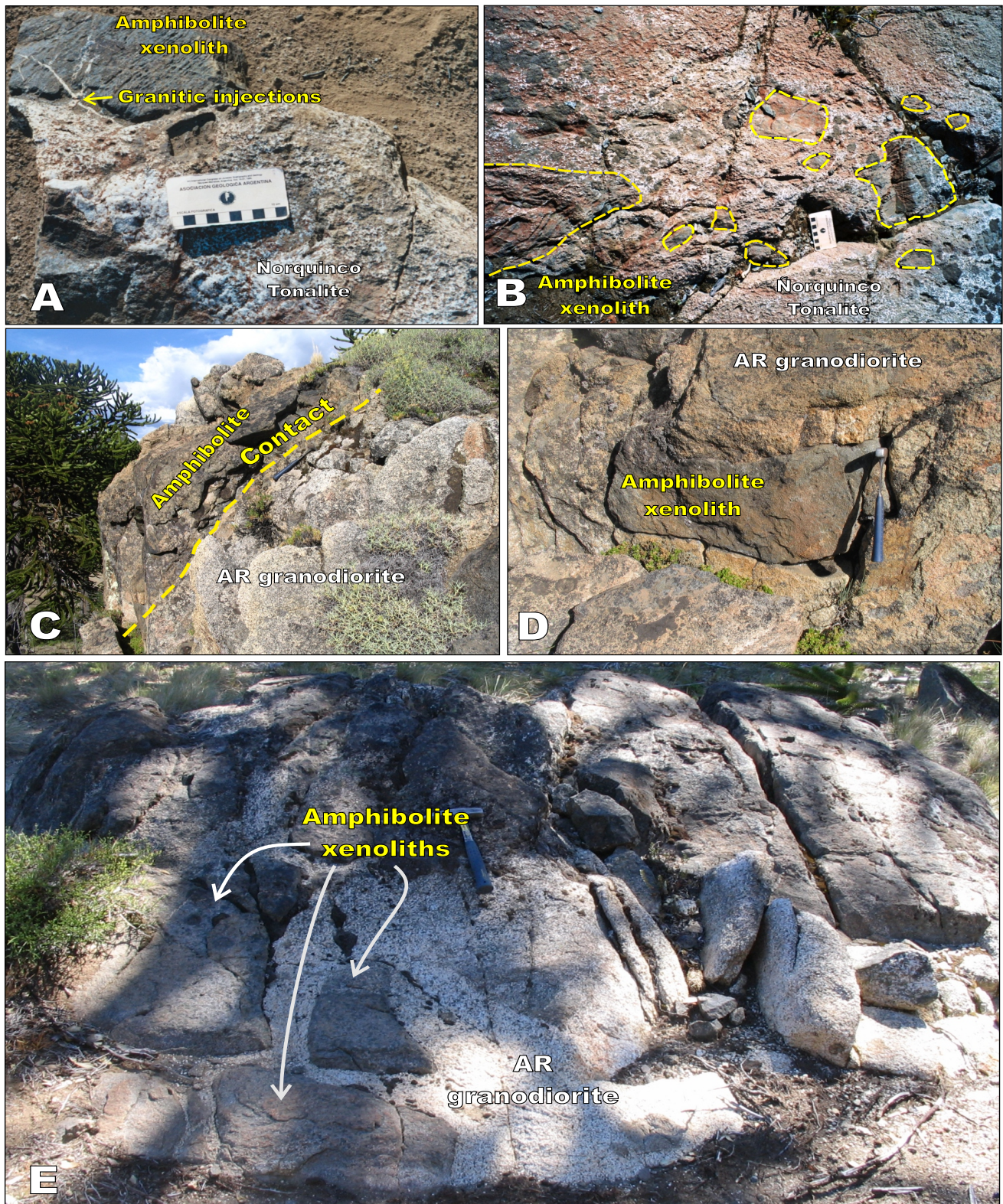


FIGURE 3. Amphibolite xenoliths in tonalites and granodiorites. A) Amphibolite xenoliths in Norquingo tonalite. Note a discordant vein from the tonalite cutting the foliation of the xenolith. B) Abundant amphibolite xenoliths in Norquingo tonalites. Note different sizes, shapes and preservation of the metamorphic structure in amphibolite xenoliths. C, D) Centimeter to meter scale blocks of amphibolite xenoliths included in Arroyo Relem granodiorites. E) Rounded amphibolite xenoliths in Arroyo Relem granodiorites. Granodioritic melt intrudes and partially assimilates “*in situ*” amphibolite forming part of the country rocks. AXG: Granodiorites-tonalites containing Amphibolite Xenoliths. AX: Amphibolite Xenoliths.

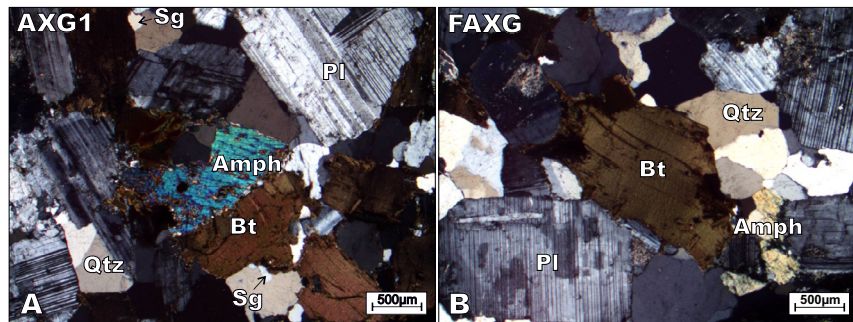


FIGURE 4. Texture and mineralogy of AXG and FAXG in thin section.

It shows strong pleochroism between olive green and pale brown. Biotite forms euhedral and subhedral prismatic crystals from more than 1mm up to 4mm long. They show red-brown pleochroism.

GEOCHEMISTRY

Determination of major elements was performed at the Activation Laboratories *ActLabs*® (Canada) using the Lithium metaborate/tetraborate fusion for ICP (code 4B) and ICP-MS (code 4B2). Samples were fused with a flux of lithium tetraborate in an induction furnace. The molten melt was immediately poured into a solution of 5% nitric acid containing an internal standard, and mixed continuously until completely dissolved (~30 minutes). For major elements, the samples were run on a combination simultaneous/sequential Thermo Jarrell-Ash ENVIRO II ICP or a Varian Vista 735 ICP. Calibration is performed using seven prepared USGS and CANMET certified reference materials. One of the seven standards is used during the analysis for every group of ten samples. For trace elements determination, fused samples

were diluted and analyzed by Perkin Elmer Sciex ELAN 6000, 6100 or 9000 ICP/MS.

Amphibolites

TiO₂ contents of 1.89wt% (Table 1) in the Ñorquinco amphibolites constitute a first diagnostic characteristic feature of an igneous origin for these rocks (Misra, 1971). On the other hand, Shaw and Kudo (1965) proposed three formulations based in various trace and major elements content, but points out that x1 is the most reliable to use since it uses less mobile elements in its formulation: $X_1 = -2.69 \log Cr - 38 \log V - 1.25 \log Ni + 10.57 \log Co + 7.73 \log Sc + 7.54 \log Sr - 1.95 \log Ba - 1.99 \log Zr - 19.58$. Positive values are indicative of ortho-amphibolites and negative values of para-amphibolites. This formulation applied to Ñorquinco amphibolites gave positive result, supporting an igneous protolith.

The Ñorquinco amphibolite Rare Earth Element (REE) pattern normalized to chondrite (Fig. 5A) is characterized by a flat pattern slightly depleted in Light REE (LREE) and

TABLE 1. Whole rock geochemistry of the amphibolites and igneous rocks containing xenoliths of amphibolites (AXG1 and AXG2) and igneous rocks lacking xenoliths (FAXG)

Sample	Amph	AXG1	AXG2	FAXG	Amph	AXG1	AXG2	FAXG	Amph	AHR	GAX	FAXG	chondrite*		
SiO ₂	47.94	64.31	67.71	66.98	Th	0.27	3.26	11.2	15	La	5.39	14.1	15.2	83.9	0.31
TiO ₂	1.89	0.497	0.332	0.436	Pb	5	16	52	23	Ce	15.9	30.3	31.1	149	0.808
Al ₂ O ₃	14.02	16.05	14.85	15.91	Ga	18	21	18	24	Pr	2.55	3.4	3.43	13.6	0.122
FeO	12.26	5.25	3.28	4.27	Zn	170	60	43	74	Nd	14	15.1	14.1	49	0.6
MnO	0.217	0.115	0.07	0.068	Cu	30	10	0	10	Sm	4.61	3.8	2.27	6.31	0.195
MgO	7.25	2.5	1.69	0.61	Ni	0	20	0	20	Eu	1.63	1.28	0.781	1.97	0.073
CaO	10.35	5.09	3.73	4.08	V	407	96	70	27	Gd	6.39	3.86	2.12	3.8	0.259
Na ₂ O	2.22	3.08	3.38	3.73	Cr	190	40	24	20	Tb	1.22	0.71	0.35	0.58	0.047
K ₂ O	0.45	1.39	2.92	1.66	Hf	3.4	2.6	2.5	12	Dy	8.34	4.36	2.01	3.2	0.322
P ₂ O ₅	0.22	0.18	0.11	0.13	Cs	0.4	3.1	2.1	4	Ho	1.73	0.81	0.4	0.63	0.072
LOI	0.74	0.91	0.91	1.37	Sc	45	16	8	31	Er	5.07	2.35	1.23	1.91	0.21
Total	97.56	99.372	98.98	99.244	Ta	0.16	0.63	0.57	1	Tm	0.742	0.345	0.186	0.289	0.032
Ba	86	240	368	192	Co	39	13	9	3	Yb	4.51	2.3	1.27	2.07	0.209
Rb	9	52	73	75	Be	1.13	3	2	2	Lu	0.663	0.373	0.223	0.377	0.032
Sr	146	244	476	222	U	2	1.29	5.05	2	Eu*/Eu					
Y	43.5	22.3	10.6	16.5	W	nd	0.9	0.7	1	La/Yb					
Zr	113	88	69	442	Ge	nd	1.6	1.6	2						
Nb	2.7	6.8	3.6	10.8	Tl	nd	0.47	0.74	1						

* values from Boynton (1984)

a Heavy REE (HREE) plateau, with a La/Yb ratio of around 1.20. Compared to the Mid-Ocean Ridge Basalt (MORB) (e.g. Pearce, 1983) (Fig. 5B), the amphibolite REE pattern show a sub-parallel trend with a general enrichment in total REE and a slightly more pronounced Eu anomaly ($\text{Eu}/\text{Eu}^* = 0.91$) suggesting a mid-ocean ridge setting for the basaltic protholiths of the amphibolites. This is also suggested by plots using immobile (Fig. 5B, C, D) (Meschede, 1986; Pearce and Cann, 1973; Pearce, 1983).

Granodiorites and tonalities

The REE patterns of three representative samples of tonalitic-granodioritic plutonic rocks from Ñorquinco

lake area are shown in Figure 6. Two of them contain abundant amphibolite xenoliths (AXG1 and AXG2), whereas a third one lacks mafic inclusions (FAXG). AXG1 and AXG2 are slightly depleted in LREE. The three samples do not show Eu anomaly (Fig. 6A; Table 1). The FAXG have a similar MREE-HREE pattern, but shows a considerable enrichment in LREE compared to AXG samples (Fig. 6A). Figure 6B shows the fields corresponding to the patterns obtained for granodiorites and tonalites belonging to the entire AIMC (Urraza *et al.*, 2011). The main difference between tonalites and granodiorites of the Ñorquinco lake area containing amphibolite xenoliths and those of the entire AIMC lacking mafic inclusions is the depletion in LREE and

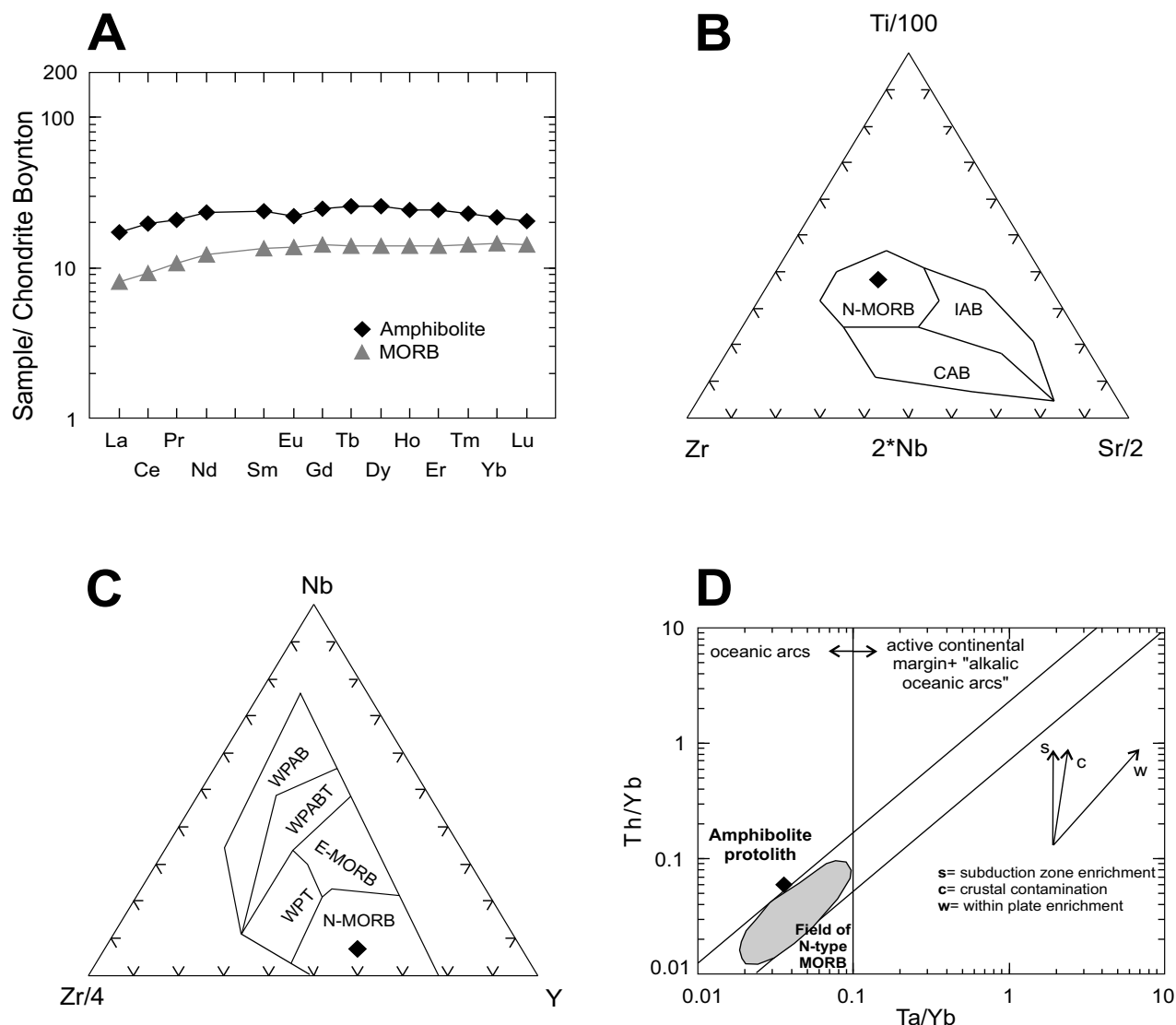


FIGURE 5. A) Amphibolite REE pattern normalized to chondrite (Boynton, 1984), compared with the typical MORB pattern. B) Zr-Ti-Sr discrimination diagram for basaltic rocks (Pearce and Cann, 1973). IAB: Island Arc Basalts; CAB: Calc-Alkaline Basalts; N-MORB: Normal Mid Ocean Ridge Basalts. C) Zr-Nb-Y discrimination diagram for basaltic rocks from Meschede (1986). WPAB: Within Plate Alkali Basalts; WPABT: Within-Plate Alkali Basalts and Within-Plate Tholeiites; E-MORB: enriched mid ocean ridge basalts; N-MORB: normal mid ocean ridge basalts; WPB: within-plate tholeiites and volcanic arc basalts. D) Th/Yb vs. Ta/Yb discriminant diagram of Pearce (1973).

TABLE 2. Representative microprobe analyses of calcic and ferromagnesian amphiboles from amphibolites. Formula based in 23 oxygens and Σ -Na-K-Ca= 13 cations (following Appendix 2, Holland and Blundy, 1994 stoichiometry) for calcic amphiboles and based on 23 oxygen and 15 cations

Ca-Amphiboles Mineral	Rims				Cores			
	rim1	rim3	core5	core6	core9	core10	core11	core17
Analyses	484	486	492	493	505	506	510	516
SiO ₂	45.7	44.24	49.6	48.97	49.18	47.82	47.57	49.82
TiO ₂	1.03	1	0.973	1.094	0.975	0.614	0.992	0.761
Al ₂ O ₃	9.76	11.74	5.96	6.46	6.19	6.7	6.62	5.75
FeO*	17.19	17.79	17.9	17.64	16.2	16.46	16.4	16.9
MgO	9.7	9.62	12.22	11.95	12.06	11.64	11.71	12.07
MnO	0.28	0.28	0.8	0.34	0.266	0.298	0.27	0.279
CaO	10.7	11	10.88	10.5	10.85	10.78	11.08	11.03
Na ₂ O	1.26	1.185	0.857	0.522	0.745	0.452	0.551	0.666
K ₂ O	0.57	0.596	0.338	0.368	0.297	0.21	0.348	0.276
Sum	96.19	97.51	98.72	97.84	96.76	94.97	95.54	97.55
Formula according Holland and Blundy (1994)								
T-sites								
Si	6.845	6.552	7.213	7.196	7.263	7.207	7.141	7.314
Al ^{iv}	1.155	1.448	0.787	0.804	0.737	0.793	0.859	0.686
Al(total)	1.723	2.05	1.022	1.119	1.078	1.190	1.172	0.995
M1,2,3 sites								
Al ^{vi}	0.569	0.602	0.235	0.315	0.34	0.397	0.313	0.309
Ti	0.116	0.118	0.106	0.121	0.108	0.07	0.112	0.084
Fe ³⁺	0.367	0.502	0.312	0.197	0.204	0.216	0.255	0.209
Mg	2.165	2.123	2.648	2.617	2.654	2.614	2.62	2.641
Mn	0.036	0.034	0.099	0.042	0.033	0.038	0.034	0.035
Fe ²⁺	1.747	1.62	1.6	1.708	1.66	1.665	1.667	1.722
M4 site								
Fe	0.039	0.082	0.166	0.263	0.137	0.194	0.138	0.144
Ca	1.717	1.746	1.695	1.653	1.717	1.741	1.782	1.735
Na	0.244	0.173	0.138	0.084	0.146	0.066	0.08	0.121
A site								
Ca	0	0	0	0	0	0	0	0
Na	0.122	0.167	0.103	0.065	0.067	0.066	0.081	0.069
K	0.109	0.13	0.063	0.069	0.056	0.04	0.067	0.052
Sum cations	15.23	15.28	15.166	15.134	15.123	15.107	15.147	15.12

Fe-Mg Amphiboles			
Mineral	Rel1	Rel2	Rel3
Analyses			
SiO ₂	51.06	51.88	51.87
TiO ₂	0.16	0.09	0.074
Al ₂ O ₃	1.15	0.72	0.553
FeO	23.15	24.45	24.32
MnO	0.73	0.78	0.771
MgO	14.91	15.26	15.05
CaO	1.46	1.25	1.209
Na ₂ O	0.09	0.09	0.067
K ₂ O	0.01	0	0.01
H ₂ O*	2	2.04	2.03
Total			
No. of oxygens	23	23	23
Structural formulae			
Si	7.85	7.89	7.91
Al ^{iv}	7.86	0.11	0.09
Al ^{vi}	0.129	0.053	0.067
Ti	0.006	0.013	0.013
Cr	0	0	0
Fe ³⁺	1.291	1.333	1.336
Fe ²⁺	1.47	1.52	1.52
Mn	0.09	0.1	0.1
Mg	3.145	3.172	3.148
Ca	0.23	0.2	0.19
Na	0.03	0.03	0.02
K	0	0	0
OH*	2	2	2

the absence of the Eu anomaly (Fig. 6A, B). These differences may be due to the assimilation of considerable amount of mafic components from the xenoliths by the granodioritic-tonalitic magma.

MINERAL CHEMISTRY

Microprobe analyses in amphiboles and plagioclase were performed with an electron microprobe JEOL JXA8900 RL at the University of Alberta. The electron beam was set at 20kV/20nA and the matrix ZAF corrections were applied. Standards were run in natural silicates (forsterite, chromite, hematite, diopside and orthoclase) with conventional procedures.

Amphiboles

Representative chemical compositions of analyzed amphiboles from Ñorquinco lake amphibolites are showed in Table 2. Mineral formulas for calcic amphiboles were calculated on the basis of 23 oxygens and $\Sigma\text{-Na-K-Ca}=13$ cations, following appendix B of Holland and Blundy (1994) stoichiometry. The ferromagnesian amphiboles were calculated based in 15eNK following Schumacher (1991). According to Leake *et al.* (1997) classification, it is possible to differentiate amphiboles according to their cation relationships: Mg-Fe amphiboles with $(\text{Ca}+\text{Na})_B < 1$ and calcic amphiboles with $\text{Ca}(\text{B}) > 1.5$. An additional condition for ferromagnesian amphiboles is the proportion of $(\text{Mg,Fe,Mn,Li})_B \geq 1.00$. The Mg/

(Mg+Fe) vs. the TSi diagram allows to classify Ca-amphibole as Mg-Hornblende for core compositions, (TSi= 6.8-7.3 i.p.f.u and Mg#= 0.55-0.8 i.p.f.u, Fig. 7A) and Tschermarkitic-Hbl for rim compositions (TSi= 6.4-6.5 i.p.f.u and Mg#~0.65). Because there is no possibility to differentiate petrographically or chemically between Mg-Fe clino and ortho-amphibole in the studied samples, the classification for clinoamphiboles was used. Cummingtonite is the most suitable phase in metabasites in low to intermediate pressures. On the basis of previous considerations, the composition of amphiboles analyzed in granodiorites is summarized as follow: Fe-Mg amphiboles have TSi~7.7 and Mg#~0.68 (Fig. 7C). Ca-amphiboles of Ñorquinco granodiorites (FAXG) classify as Mg-hornblende (TSi between 6.3-6.8 and Mg#~0.65, Fig. 7B). A cummingtonite composition with Mg#=0.65-0.67 and TSi between 7.41-7.61 i.p.f.u was found for the AXG amphiboles (Table 2; Fig. 7D). It is important to highlight this fact, given that Andean calc-alkaline igneous rocks are characterized primarily by Ca-amphiboles, whereas Fe-Mg-amphiboles are extremely rare in this setting.

Plagioclase

Plagioclase varies in composition from andesine to labradorite (An_{41-57}) (Fig. 7E). The plagioclase of AXG1 is calcic to intermediate with An_{36} to An_{52} contents (Fig. 7F), whereas the compositions of AXG2 and FAXG plagioclases varies between oligoclase and andesine (An_{28-50}) (Fig. 7G, H) (Table 3):

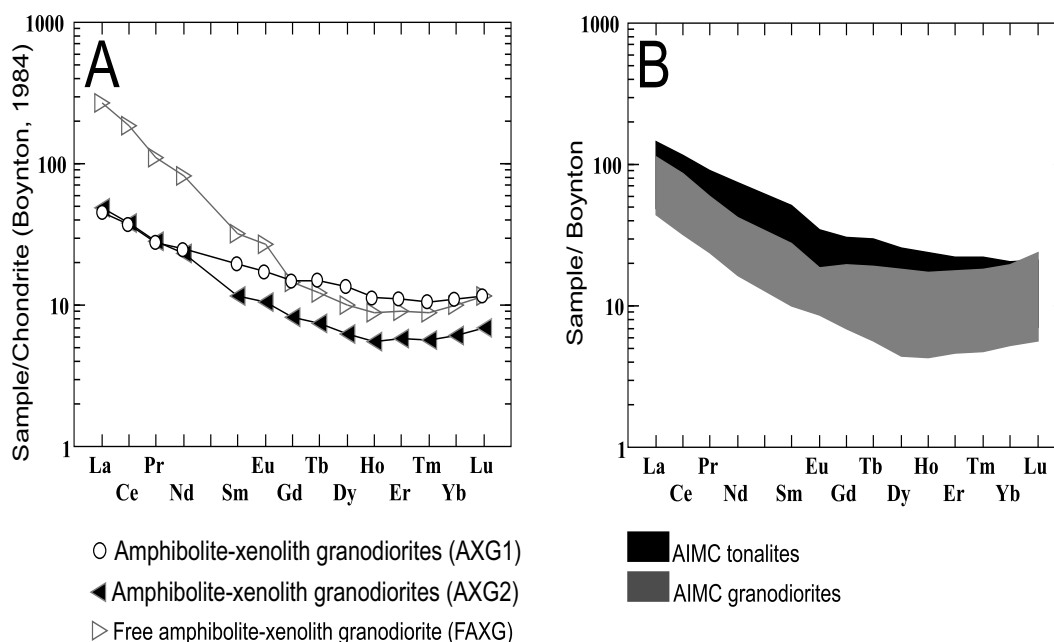


FIGURE 6. A) REE pattern normalized to chondrite (Boynton, 1984) of granodiorites with (AXG1 and AXG2) and without (FAXG) amphibolite xenoliths. B) Fields of REE patterns for granodiorites and tonalites of the entire AIMC (from Urraza *et al.* 2011).

TABLE 3. Representative microprobe analyses of plagioclases from amphibolites

Sample	Amphibolites			AXG1			AXG2			FAXG		
	0826PI1	0826PI2	0826 PI3	295	298	300	191	195	226	347	351	352
SiO ₂	55.95	54.71	56.14	57.39	58.82	56.07	58.39	57.84	57.44	60.29	60.00	61.43
TiO ₂	0	0	0	0	0	0	0	0.015	0.025	0.011	0	0
Al ₂ O ₃	28.51	28.76	27.80	26.50	25.43	27.90	26.42	26.67	26.31	25.42	25.22	24.61
FeO	0.113	0.163	0.146	0.198	0.181	0.086	0.213	0.19	0.191	0.073	0.059	0.039
MnO	0	0	0.02	0	0.01	0	0	0	0	0	0.024	0
MgO	0	0.01	0	0.01	0.019	0.015	0.011	0	0.011	0.024	0.013	0.015
CaO	10.77	10.8	9.53	8.62	7.4	10.05	8.11	8.57	8.31	7.07	7.2	6.38
Na ₂ O	5.33	5.14	5.60	6.37	7.02	5.58	6.84	6.73	6.66	7.42	7.50	7.85
K ₂ O	0.076	0.108	0.101	0.186	0.236	0.13	0.265	0.254	0.235	0.236	0.162	0.356
Total	100.75	99.68	99.34	99.27	99.12	99.83	100.25	100.27	99.18	100.54	100.18	100.68
Si	9.994	9.889	10.134	10.355	10.593	10.090	10.430	10.350	10.380	10.690	10.680	10.850
Al	5.997	6.121	5.910	5.631	5.394	5.913	5.557	5.618	5.598	5.305	5.287	5.121
Fe ²⁺	0.017	0.025	0.022	0.03	0.027	0.013	0.032	0.028	0.029	0.011	0.009	0.006
Mn	0	0	0.003	0	0.002	0	0	0	0	0	0.004	0
Mg	0	0.003	0	0.003	0.005	0.004	0.003	0	0.003	0.006	0.003	0.004
Ca	2.061	2.091	1.843	1.666	1.428	1.938	1.552	1.643	1.609	1.342	1.373	1.208
Na	1.844	1.800	1.960	2.229	2.451	1.947	2.369	2.334	2.333	2.550	2.589	2.689
K	0.017	0.025	0.023	0.043	0.054	0.03	0.06	0.058	0.054	0.053	0.037	0.08
Ab	47	46	51.2	56.6	62.3	49.7	59.5	57.8	58.4	64.6	64.7	67.6
An	52.5	53.4	48.2	42.3	36.3	49.5	39	40.7	40.3	34	34.3	30.4
Or	0.4	0.6	0.6	1.1	1.4	0.8	1.5	1.4	1.4	1.3	0.9	2

GEO-THERMOBAROMETRY

Conventional geothermobarometry and textural relationships

Pressure conditions were estimated in Ca-amphiboles using the Al-in-Hbl formulation of [Johnson and Rutherford \(1989\)](#), corrected by temperature by [Anderson and Smith \(1995\)](#), which has been widely applied to different lithologies ([Table 4](#)) and the Ti-Al in Ca-amphibole of [Ernst and Liu \(1998\)](#). The temperature conditions were calculated using the latter thermobarometer and the Hbl-Pl thermometer of [Holland and Blundy \(1994\)](#). The $T_{B(ed-rich)}$ formulation calibrated for associations with or without quartz was considered as the most appropriate for the observed mineral associations. Conventional geothermobarometry results obtained in Ñorquinco amphibolites are shown in [Table 4](#) and the P-T points are shown as stars in [Figure 8](#). The cores yield in the range 677–745°C using TB and 646°–680°C using Ti-Al in Hbl, while the rims yield slightly higher temperatures (723°C using TB and 684–687°C using the Ti in Hbl thermometer, [Otten, 1984](#)). Despite the variation between the results obtained using both thermometers are less than 50°C, a coherent correlation between both supports analytical calculations. Although from these calculations a difference between cores and rims is detected, the greatest is obtained by applying geobarometers. The [Anderson and Smith \(1995\)](#) geobarometer applied to Ñorquinco amphibolites yield 1.87 to 3.9kbar for the cores and 6.40kbar for the rims, showing a difference of ~2.5kbar between both

stages. Similar pressure changes are calculated with the Ti-Al in Hbl thermobarometer ([Fig. 9](#)).

Pseudosection and metamorphic path

In order to evaluate the stability of the mineral associations in amphibolites, a P-T pseudosection was built using the program *Perplex_X* ([Connolly, 1990, updated version 2015](#)). The diagram was made using a representative whole-rock chemistry of amphibolites, considering the chemical system Na₂O-CaO-FeO-MgO-Al₂O₃-SiO₂-K₂O-H₂O and including the following phases: plagioclase, olivine, orthopyroxene, clinopyroxene, amphibole, orthoamphibole, biotite, garnet, chlorite, actinolite and water (1.5%). The [Holland and Powell \(1998, updated version hp02ver\)](#) internally consistent thermodynamic data set was applied using the solid solution models given by: [Holland and Powell \(1998\)](#) for olivine, clinopyroxene, orthopyroxene, garnet, biotite, melt and chlorite, [Newton *et al.* \(1981\)](#) for plagioclase, [Dale *et al.* \(2005\)](#) for Ca-amphibole, [Diener \(2007\)](#) for clinoamphibole and [Massonne and Willner \(2008\)](#) for actinolite. In the P-T pseudosection ([Fig. 8](#)) the observed association in amphibolites (Camp+Ca-Amp+Pl+Bt+Qz+Ilm+H₂O), is restricted to the temperature between 570–740°C at 2kbar and 700–770°C at 5.5kbar. The appearance of Opx predicted by the model at higher temperatures and which is not present in the studied rocks fixes the maximum temperatures of stability for this first association. Similarly, the upper pressure limit for this association is determined by the predicted appearance of Grt, absent from these rocks. The presence of ferromagnesian amphibole as a relict phase and compositional variations in Ca-amphibole

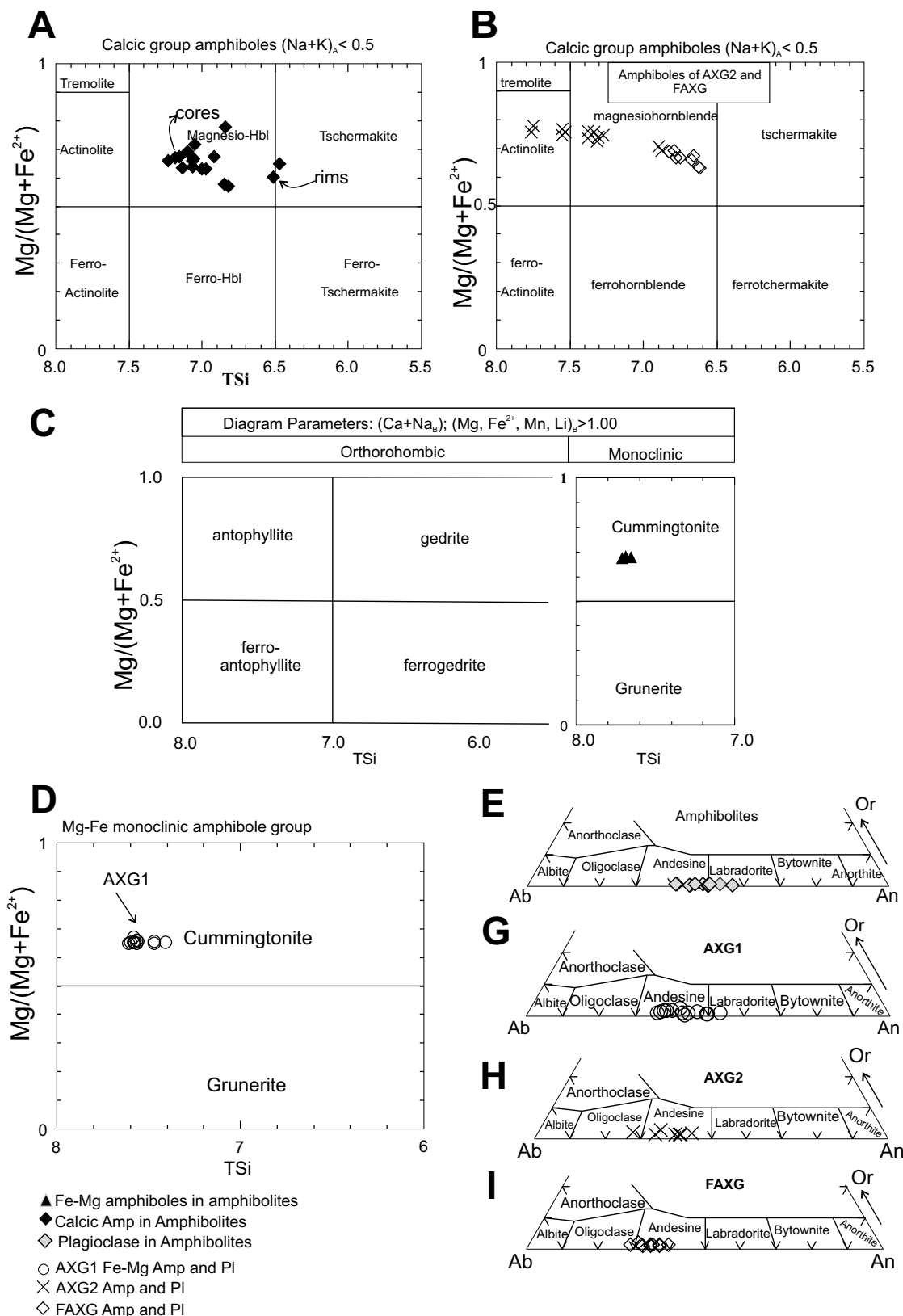
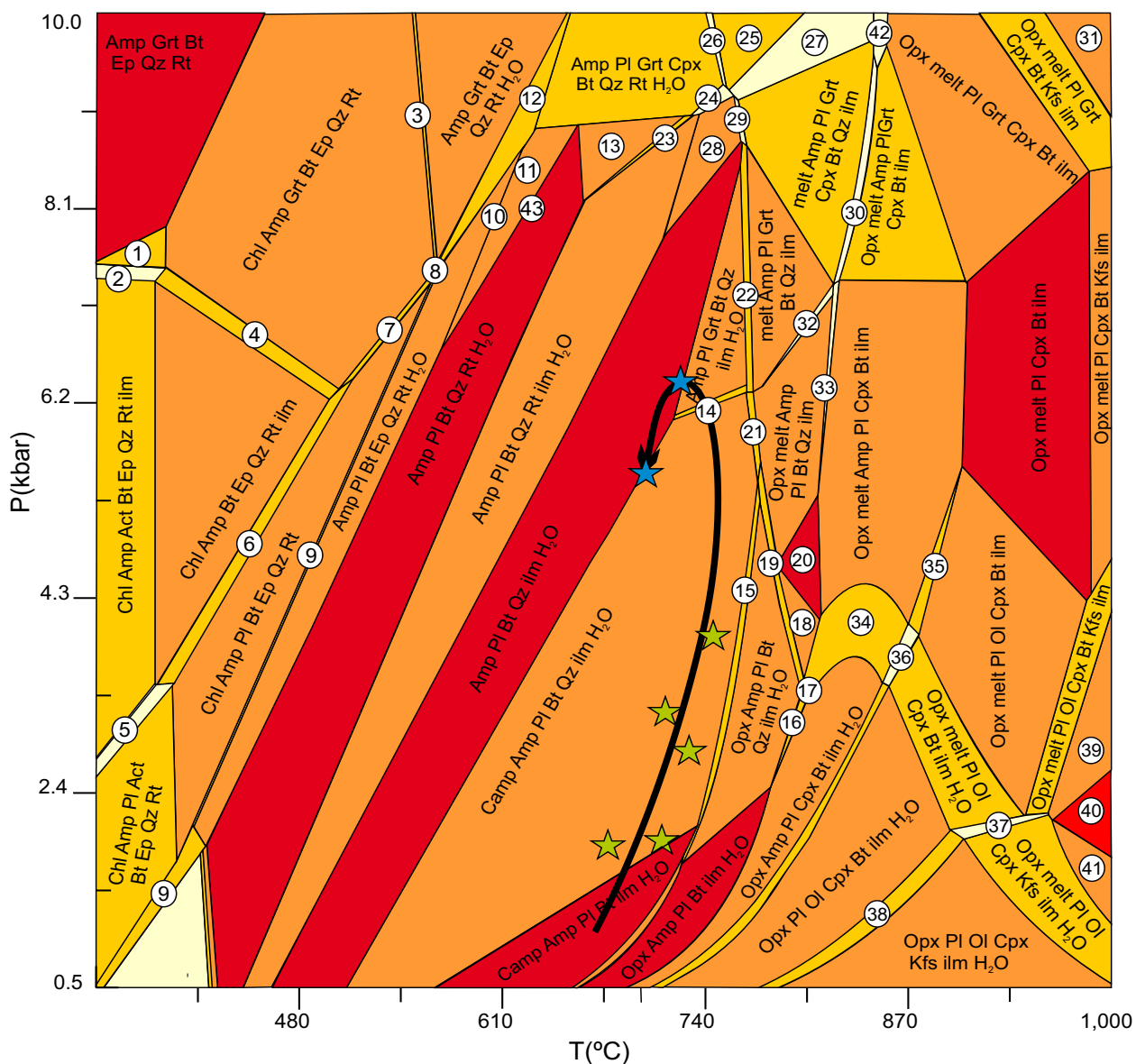


FIGURE 7. Leake et al. (1997) classification of amphiboles from amphibolites and granodiorites-tonalites. A) Classification of Ca-amphiboles from Ñorquinco amphibolites. B) Ca-amphiboles from AXG2 and FAXG. C) Classification of relict Mg-Fe amphiboles in Ñorquinco amphibolites. D) Classification of Mg-Fe amphiboles of AXG1 and E) Ternary An-Ab-Or classification diagram for feldspars in AXG1, AXG2 and FAXG amphibolites (Deer et al., 1966 and references therein).



- | | | |
|---|---|---|
| 1-Chl Amp Grt Act Bt Ep Qz Rt | 15-Opx Camp Amp PI Bt ilm H ₂ O | 29-melt Amp PI Grt Cpx Bt Qz ilm H ₂ O |
| 2-Chl Amp Grt Act Bt Ep Qz Rt ilm | 16-Opx Amp PI Cpx Bt Qz ilm H ₂ O | 30-Opx melt Amp PI Grt Cpx Bt Qz ilm |
| 3-Chl Amp Grt Bt Ep Qz Rt H ₂ O | 17-Opx melt Amp PI Cpx Bt Qz ilm H ₂ O | 31-Opx melt PI Grt Cpx Kfs ilm |
| 4-Chl Amp Grt Bt Ep Qz Rt ilm | 18-Opx melt Amp PI Bt ilm H ₂ O | 32-Opx melt Amp PI Grt Bt Qz ilm |
| 5-Chl Amp PI Act Bt Ep Qz Rt ilm | 19-Opx melt Amp PI Bt Qz ilm H ₂ O | 33-Opx melt Amp PI Cpx Bt Qz ilm |
| 6-Chl Amp PI Bt Ep Qz Rt ilm | 20-Opx melt Amp PI Bt ilm | 34-Opx melt Amp PI Cpx Bt ilm H ₂ O |
| 7-Chl Amp PI Grt Bt Ep Qz Rt | 21-Camp melt Amp PI Bt Qz ilm H ₂ O | 35-Opx melt Amp PI OI Cpx Bt ilm |
| 8-Chl Amp PI Grt Bt Ep Qz Rt H ₂ O | 22-melt Amp PI Grt Bt Qz ilm H ₂ O | 36-Opx melt Amp PI OI Cpx Bt ilm H ₂ O |
| 9-Amp PI Act Bt Ep Qz Rt H ₂ O | 23-Amp PI Grt Bt Qz Rt ilm H ₂ O | 37-Opx melt PI OI Cpx Bt Kfs ilm H ₂ O |
| 10-Chl Amp PI Bt Ep Qz Rt H ₂ O | 24-Amp PI Grt Cpx Bt Qz Rt ilm H ₂ O | 38-Opx PI OI Cpx Bt Kfs ilm H ₂ O |
| 11-Amp PI Cpx Bt Qz Rt H ₂ O | 25-melt Amp PI Grt Cpx Bt Qz Rt | 39-Opx melt PI OI Cpx Kfs ilm |
| 12-Amp PI Grt Bt Ep Qz Rt H ₂ O | 26-melt Amp PI Grt Cpx Bt Qz Rt H ₂ O | 40-melt PI OI Cpx Kfs ilm |
| 13-Amp PI Grt Bt Qz Rt H ₂ O | 27-melt Amp PI Grt Cpx Bt Qz Rt ilm | 41-melt PI OI Cpx Kfs ilm H ₂ O |
| 14-Camp Amp PI Grt Bt Qz ilm H ₂ O | 28-Amp PI Cpx Bt Qz ilm H ₂ O | 42-Opx melt Amp PI Grt Cpx Bt Rt ilm |
| | | 43-Amp PI Cpx Bt Ep Qz Rt H ₂ O |

FIGURE 8. P-T pseudosection for the MORB derived amphibolites of the AIMC. Stars represent the P-T points calculated using conventional geothermobarometry. Thick solid line represents the calculated trajectory. Dotted curve is the estimated trajectory according to the mineral assemblage.

from cores to rims, evidence changes of the P-T conditions. These changes lead to the formation of the association Amp+Pl+Bt+Qz+Ilm+H₂O, stable in the contiguous field to lower temperature where clino-amphibole is not stable (Fig. 8).

Pseudosection analysis was complemented with the application of conventional geothermobarometry previously shown. Green stars in Figure 8 are P-T conditions calculated using mineral core compositions. Obtained temperatures are in the range 677–745°C and pressures vary between 1.9–3.9kbar (adjusted with T_B). Blue stars in Figure 8 represent P-T conditions obtained with rim compositions. Internal rim composition gives a temperature of 724°C and a pressure of 6.4kbar, whereas for the outer part of the rim yield a temperature of 702°C and a pressure of 5.5kbar were obtained (Table 4). Geothermobarometric results indicate that Ca-amphibole continued to form after the accretion of mafic bodies at very low pressures (recorded by relict Fe-Mg-amphibole), and during the path toward conditions of increasing pressure, as indicated by its distribution in Figure 8. On the other hand, edges record the evolution between the peak pressure achieved and the final equilibration, allowing to define the retrograde part of a counterclockwise trajectory (Fig. 8).

Chemical exchanges in Ca-amphiboles and isopleths modeling

It is well known that the compositional variability of Ca-amphiboles with the change in the physical conditions are

related mainly to Fe-Mg (Fe=Mg), edenitic (NaAl^{IV}=oSi), tschermakitic (MgSi=Al^{IV}Al^{VI} or FeSi=Al^{IV}Al^{VI}) and pargasitic (NaAl^{VI}Al^{IV}=oMgSi₂) exchanges (Spear 1993, en references therein). It has been established through numerous experimental and empirical studies that Al replaces Si in tetrahedral coordination in Ca-amphibole with increasing temperature, whereas Al substitutes for Mg and/or Fe in the M2 octahedral site and NaM4 boosts with increasing pressures (Anderson and Smith, 1995; Ernst and Liu, 1998; Gilbert *et al.*, 1982; Hawthorne, 1981; Johnson and Rutherford, 1989; Raase, 1974; Robinson *et al.*, 1982). Ti contents also boosts with increasing temperature at constant pressure, but decrease only slightly with increasing pressure at constant temperature (Ernst and Liu, 1998). These chemical variations due to changes in metamorphic conditions along the proposed P-T trajectory are recorded in the composition of cores and rims of Ca-amphibole of the studied rocks.

The most significant changes observed in the chemical analyses of Ca-amphibole cores and rims showed in Table 2, are a decrease of Mg^{M2} (from 2.65 in cores to 2.12 i.p.f.u in rims) content and an increase in the Al^{VI} (from 0.73 to 1.45) and Na^{M4} (from 0.065 to 1.16). Taking into account that an increase of Al^T (from 1.022 to 2.05) and a decrease of Si (from 7.31 to 6.55) is also observed, the most plausible interpretation for this chemical variation is a coupled tchermakitic substitution of the type MgSi=Al^{IV}Al^{VI}. In spite of the increase of the A site filled by alkalis (Na⁺-K⁺)

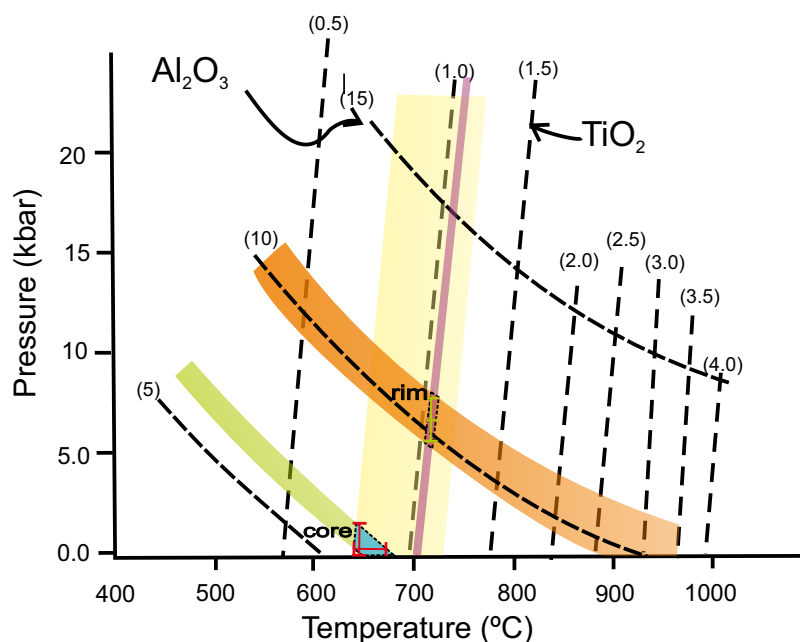


FIGURE 9. Application of the geothermobarometer Ti-Al in Ca-amphibole of Ernst and Liu (1998). Compositions. Orange area: Al₂O₃ contents of rims (between 9.7 and 11.7wt%), pink area: TiO₂ contents for rims (between 1.03 and 1.06wt%). Green area: Al₂O₃ contents range (between 5.96 and 6.7wt%) and yellow zone represent the TiO₂ contents of cores (0.76-1.09wt%). The intersection between the isopleths for Al₂O₃ and TiO₂ contents for the composition of rims and cores allow restricting the P-T conditions range.

and some contribution to the decrease in Si due to an edenitic substitution ($\text{NaAl}^{\text{IV}}=\text{oSi}$) favored by a temperature increase, the constancy in Ti content seems to indicate that the contribution of temperature to the compositional change between the two stages has not been significant compared to the influence of pressure. This pressure increase recorded by Ca-amphibole cores and rims agrees very well with the P-T path previously proposed on the basis of phase relations and conventional geothermobarometry.

Ernst and Liou (1998) calibrated a semiquantitative thermobarometer based on an experimental phase-equilibrium study of Al and Ti contents of Ca-Amphiboles synthesized from natural MORB. The result of the

application of this geothermobarometer to average cores and rims compositions of Ca-amphibole from MORB-derived amphibolites of the Ñorquinco area is showed in Figure 9. The temperature for cores is around 650–680°C, with pressure up to ~2kbar. Rims show a very restricted area for temperature (705–710°C) and pressures up to 7.5, with an average of 6.48kbars. Again, pressure change appears as the dominant factor in the compositional variation between both considered stages, with a limited contribution to temperature change.

Werami (Perplex_X package) P-T diagrams showing Ca-amphibole Si and Mg isopleths are showed in Figure 10A, B Ti cannot be modeled because this component

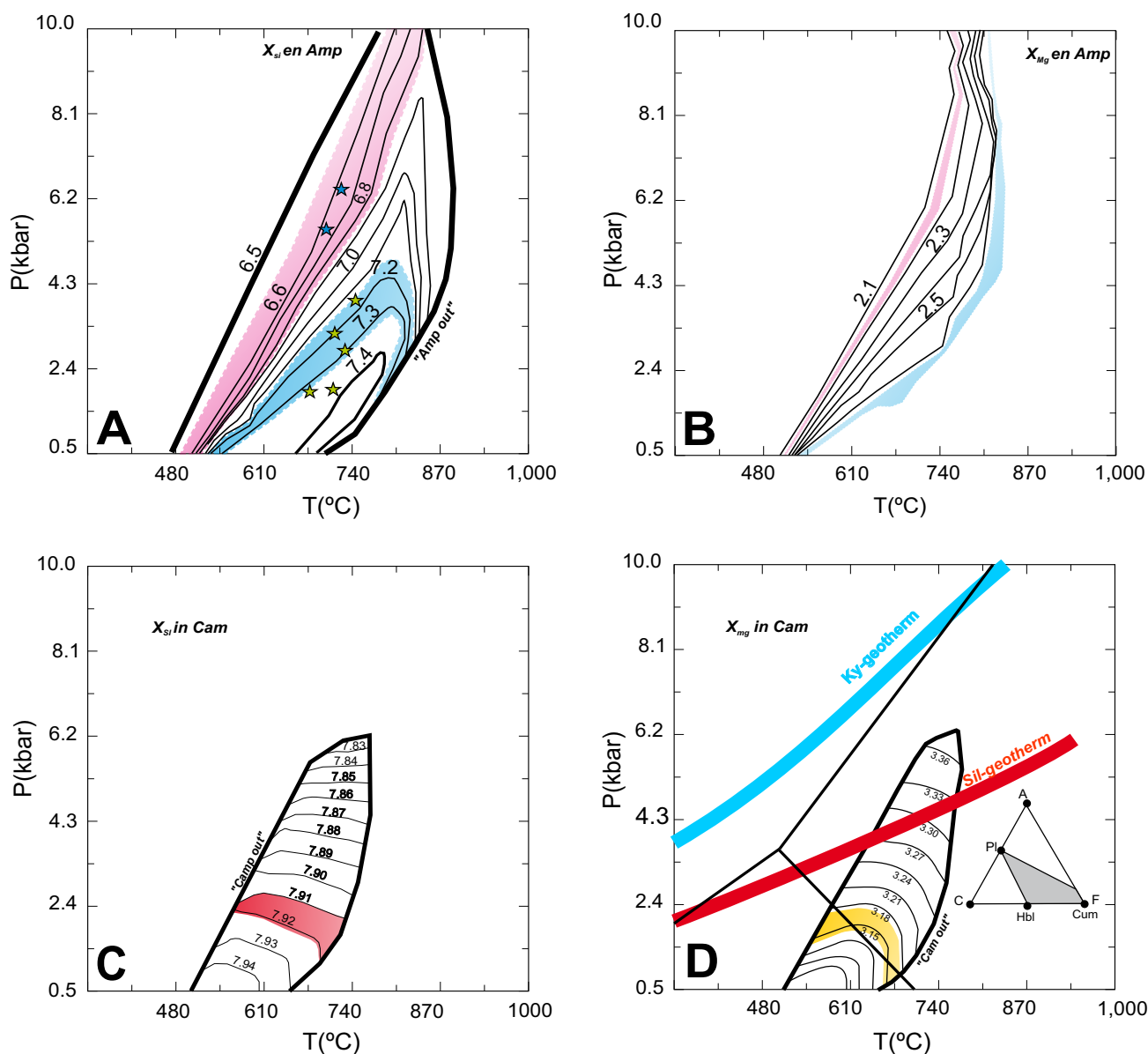


FIGURE 10. A, B) Si and Mg isopleths (i.p.f.u) for modeled Ca-amphibole using werami; green and blue stars are taken from Figure 8; C, D) Mg and Si isopleths in Fe-Mg-amphibolites from Ñorquinco amphibolites. Ky and Sil isotherms and aluminum silicates stability fields, shown for reference. AFC diagram modified from Butcher and Frey (1994). Details in the text.

is not included in the Ca-amphibole solid solution formulation of Dale *et al.* (2000), used for the construction of pseudosection. Cores and rims obtained using Al-Ti geothermobarometer of Ernst and Liou (1998) previous shown (Fig. 9) were plotted in the Si and Mg isopleths diagrams. It can be appreciated that Si and Mg contents partially confirm the results obtained through the Al-Ti geothermometer, with a small difference in the P-T values in cores.

Finally, isopleths P-T diagrams showing the stability field, Si and Mg isopleths corresponding to Mg-Fe-amphibole are presented in Figure 10C, D isopleths for Si (enhanced in red) show a stability field with temperatures up to 740°C, and pressures between 2.4–2.8, even though Mg-in-clinoamphiboles compositional range (enhanced in yellow), constrains the stability of this relict phase to temperatures in the range 550–680°C and pressures below 2.3kbar. These low pressures obtained for some Ca-amphibole cores are suggested to be the closest to those expected for the starting metamorphic conditions of these mafic rocks.

Both, chemical exchanges in Ca-amphiboles and isopleth modeling argue in favor of a counterclockwise path characterized by a considerable increase of pressure and a moderate variation of temperature, as previously proposed on the basis of pseudosection modeling and conventional geothermobarometry.

GEOCHRONOLOGY

Analytical procedures

A representative sample of “in situ” amphibolites from the Ñorquinco lake (S39°08'20"; W71°16'4") area

was dated using $^{40}\text{Ar}/^{39}\text{Ar}$ amphibole geochronology at the Noble Gas Laboratory, Pacific Centre for Isotopic and Geochemical Research, University of British Columbia, Canada. The sample was irradiated at the McMaster Nuclear Reactor in Hamilton, Ontario, for 160MWH in the medium flux site 8E. Analyses (n=85) of 19 neutron flux monitor positions produced errors of <0.5% in the J value. The mineral separates were step-heated at incrementally higher powers in the defocused beam of a 10W CO₂ laser (New Wave Research MIR10) until fused. All measurements were corrected for total system blank, mass spectrometer sensitivity, mass discrimination, radioactive decay during and subsequent to irradiation, as well as interfering Ar from atmospheric contamination and the irradiation of Ca, Cl and K (Isotope production ratios): ($^{40}\text{Ar}/^{39}\text{Ar}$) K=0.0302±0.00006, ($^{37}\text{Ar}/^{39}\text{Ar}$) Ca=1416.4±0.5, ($^{36}\text{Ar}/^{39}\text{Ar}$) Ca=0.3952±0.0004, Ca/K=1.83±0.01 ($^{37}\text{ArCa}/^{39}\text{ArK}$). Initial data entry and calculations were carried out using the software ArArCalc (Koppers, 2002). The plateau and correlation ages were calculated using Isoplot ver.3.09 (Ludwig, 2003).

Results

The separated Ca-amphibole concentrate from the MORB-derived amphibolites of the AIMC (sample 0826) displays an internally concordant isochrone of 212.7±9.6Ma (Fig. 11A; Table 5), whereas it yields an age of 208.4±9.9Ma (Fig. 11B) according to the $^{36}\text{Ar}/^{40}\text{Ar}$ vs. $^{39}\text{Ar}/^{40}\text{Ar}$ isotope correlation (Mean Square Weighted Deviation, MSWD= 1.5).

It is important to discuss the meaning of the obtained age, regarding the tectono-metamorphic events recognized in the area. At first, it is important to highlight that the diffusion coefficient is extremely sensitive to temperature. Consequently, there will be a temperature at which the system

TABLE 4. Geothermobarometric results obtained from the application of conventional formulations indicated in the text. The first column provides data about the mineral pairs that were used for pressure and temperature determinations. The second column shows the molar fraction albite in plagioclase, XAb is required for Hbl-Pl geothermometry following Holland and Blundy (1994). The third column shows Al(total) value resulting from the sum of the tetrahedral and octahedral aluminum and is used to determine the estimation of pressures applying geobarometry formulas (fourth and seventh column). The fourth column shows the values obtained by applying the barometer proposed by Johnson and Rutherford (1989). The fifth column shows the temperature values obtained using the TB formula proposed by Holland and Blundy (1994). The sixth column shows the temperature values obtained using the Ti geothermometer in hornblende (Otten, 1984). The last column shows the pressure values obtained by applying the Anderson and Smith (1995) formulation in kilobars

Sample	XAb	Al (total)	J&R(1989)	T _B (H&B)	T (C)	Ti-Hbl	A&S(1995)
Hb1-PI1	0.51	1.72	3.83	702.13	684.56	5.49	
Hb3-PI3	0.50	2.05	5.21	723.89	687.02	6.39	
Hb2-PI2	0.43	1.26	1.87	717.08	679.89	3.17	
Hb4-PI4	0.59	1.53	3.02	744.68	696.50	3.91	
Hb5-PI5	0.54	1.02	0.86	711.81	673.12	1.92	
Hb13-PI13	0.50	1.20	1.61	729.25	723.78	2.79	
Hb17-PI16	0.50	1.00	0.75	677.33	646.16	1.87	

begins to retain the radiogenic isotope for each mineral. This is called closure temperature, and for hornblende it is around 500–550°C (McDougall and Harrison, 1999). The presence of relict Fe-Mg amphiboles and the chemical zoning recognized in Ca-amphiboles denote that the MORB-derived amphibolites were subjected to at least two metamorphic events. It implies that the $^{40}\text{Ar}/^{39}\text{Ar}$ age obtained in this study does not represent the age of the oldest tectono-thermal event. This presumption is supported by the ~360Ma age obtained from U-Th/Pb in monazite of schists enclosing amphibolite lenses, interpreted as the age of the first tectono-metamorphic event of the region (Urraza *et al.*, 2009). Since the temperature calculations indicate that the second tectono-metamorphic event took place above the $^{40}\text{Ar}/^{39}\text{Ar}$ closure temperature for amphiboles, the obtained age of 212.7Ma is interpreted as a minimum for the development of this event. This age can be related to the youngest age recorded in monazite hosted in peraluminous tonalites outcropping next to Ñorquinco area, that yield a first event with average ages of 256Ma and a second event with average ages of 221Ma (Urraza *et al.*, 2009).

DISCUSSION

P-T-path and related metamorphic events

Petrographic characteristics and phase relations combined with geothermobarometry and the evaluation of the changes in the chemistry of zoned Ca-amphiboles allow us to define a counterclockwise P-T path for the evolution of the amphibolites of the Ñorquinco area.

At least two metamorphic events were recognized in amphibolites: the first one took place under low-pressure amphibolite facies and is related to a mineral association in equilibrium with relict Mg-Fe-amphibole and Ca-amphibole cores (M_1 , Fig. 12A, B). This event agrees with the first event characterized by pressures below 3.8kbar and temperatures above 620°C determined for adjacent metapelitic rocks (Urraza *et al.*, 2009). The second event (M_2) is characterized by recrystallization of amphibole and compositional changes in relict porphyroblast rims. This second overprinted event is represented by the mineral association in equilibrium with Ca-amphibole rims and small recrystallized grains located at their margins and distributed along the foliation planes. This last event took place at around 700°C and 6.4kb (Fig. 12B), and is also comparable to the second event determined by the enclosing metapelitic rocks (at least ~615–640°C at 6.2–6.7kbar) (Fig. 12A), indicating a common tectono-metamorphic evolution.

Two metamorphic events and a counterclockwise trajectory were also established for the post-emplacment

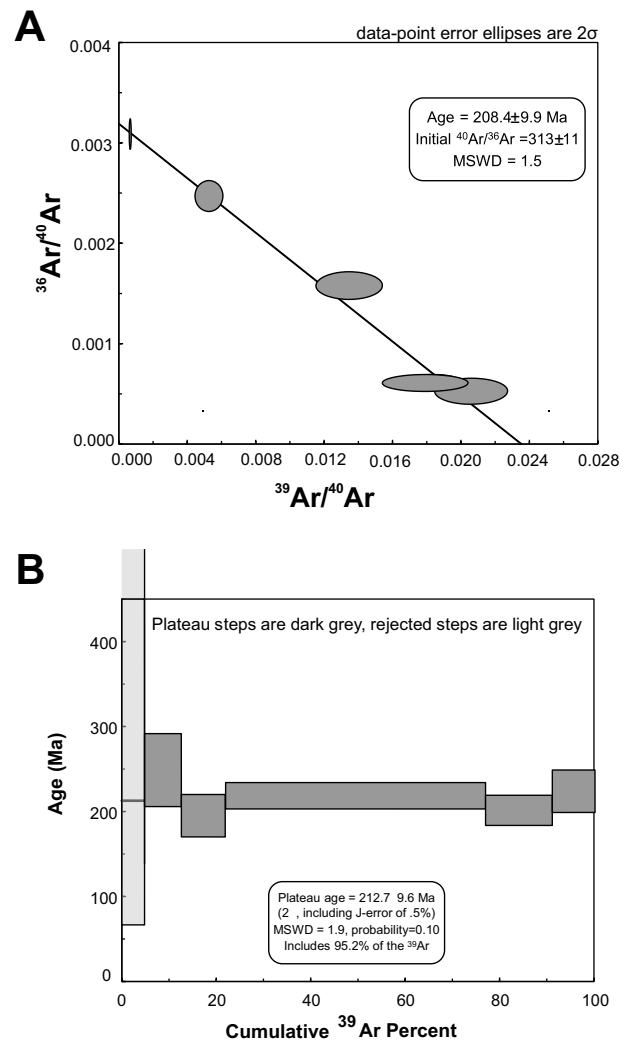


FIGURE 11. A) $^{36}\text{Ar}/^{40}\text{Ar}$ vs. $^{39}\text{Ar}/^{40}\text{Ar}$ isotope correlation in Ca-amphibole concentrates from the MORB-derived Ñorquinco amphibolites (two sigma intra-laboratory analytical uncertainties quoted). B) Plot shows age-spectra obtained from step-heating experiments versus cumulative ^{39}Ar gas released.

evolution of coronitic metatroctolites of the same area (Urraza *et al.*, 2009, 2015). In the Ñorquinco metagabbros, a P-T path following four stages (A, B, C, and D) given by different reactions show a counterclockwise trajectory similar to the amphibolite P-T path, but developed at higher temperatures. The primary-magmatic association in metatroctolites $\text{Pl}_1 + \text{Ol} + \text{Cpx}_1 + \text{Hbl}_1$ (A) was re-equilibrated during the post-emplacment thermal descent giving place to the formation of coronas around olivine crystals, with successive formation of orthopyroxene, clinopyroxene (Cpx_2), amphibole (Hbl_2) and spinel. M_1 in metatroctolites by assemblage B (4.3kbar, ~845°C), and M_2 by assemblages C (775°C, 5.8kbar) and D (694°C, ~4.5kbar), see Urraza *et al.* (2015). The age registered in metagabbro xenoliths hosted in granodiorites constrains the emplacement of mafic intrusives to the Late Carboniferous (309Ma, Urraza

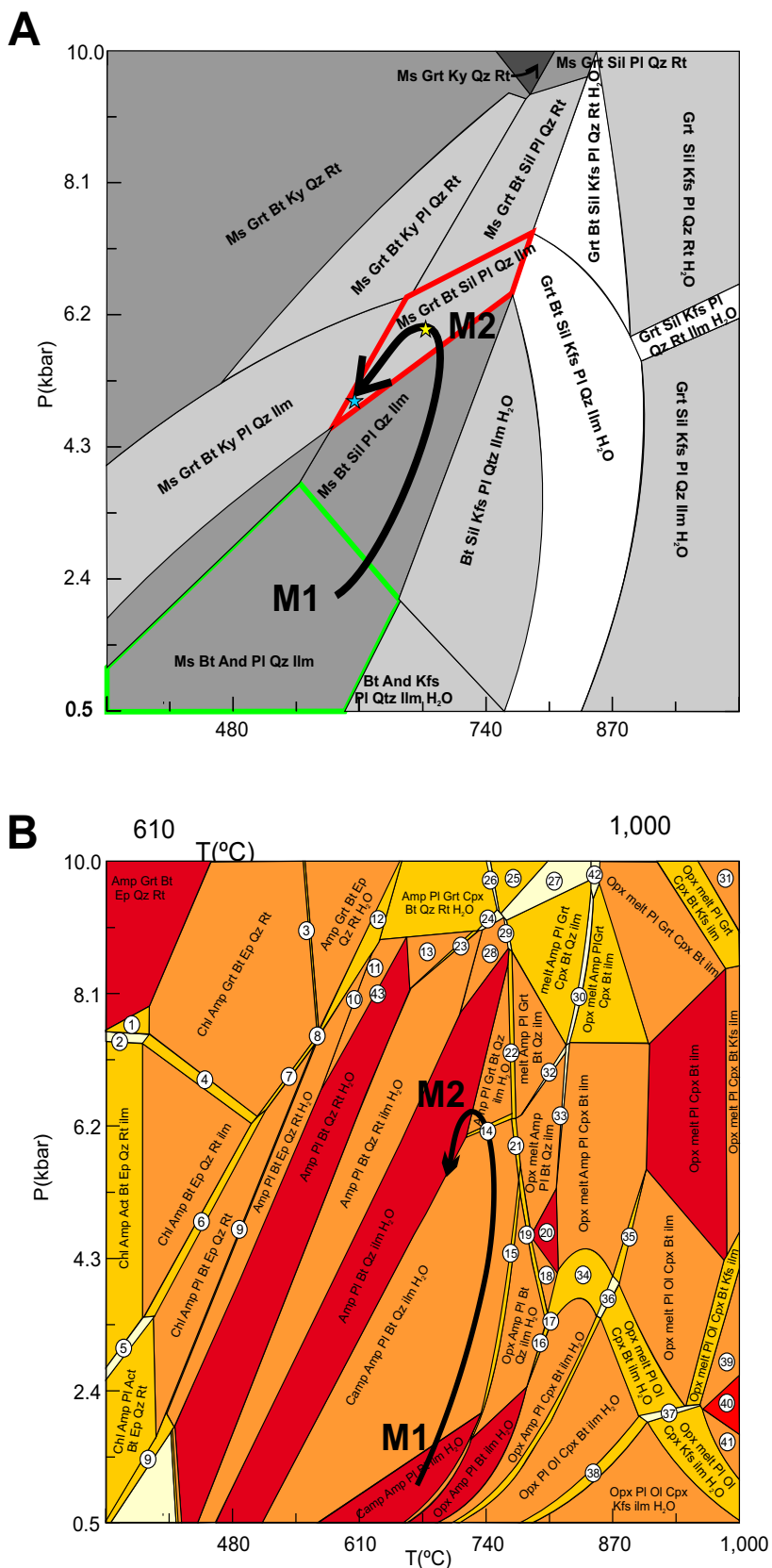


FIGURE 12. P-T path defined in the different rocks of the metamorphic accretion prism. A) Trajectory calculated in the metasedimentary rocks. Stars were calculated using conventional geothermobarometry in garnet rims (Urraza et al., 2009). B) P-T path obtained for the MORB derived amphibolites..

et al., 2015). Thus, the late Paleozoic-Triassic metamorphic evolution seems to be identical for all lithologies studied to the south of the AIMC area.

Regional correlations

The country rocks of southern AIMC and the amphibolites studied in this contribution are considered as a metamorphic sequence related to an accretionary prism developed during the Late Paleozoic-Triassic subduction along the southwestern margin of Gondwana (Urraza, 2014; Urraza *et al.*, 2015). The AIMC metamorphic sequence is composed of quartzo-feldspatic metapelites and intercalated amphibolites (Urraza *et al.*, 2008a, 2009, 2011). Most of the outcrops are constituted by intensely foliated gneisses, with injections of granitic material of the 'lit par lit' type that frequently show isoclinal and intrafoliar folding, with concordant finely foliated intercalations of amphibolites. This metamorphic sequence was intruded by Late Paleozoic magmatic bodies including granodiorites, tonalites, norites and troctolites (Urraza *et al.*, 2015, and references therein). The amphibolites studied in the present contribution, as well as other basement rocks, are present not only as "in situ" exposures, but also as variably sized xenoliths in younger tonalitic intrusives. The WNW-ESE Aluminé-Ñorquinco regional lineament system (Fig. 13) separate two different lithological-structural domains: i) The southern zone is formed by metapelites of mid Paleozoic depositional age forming an early basal accretionary prism into which MORB-derived amphibolites slices were tectonically emplaced and ii) the northern area is characterized almost exclusively by high-grade metamorphic rocks intruded only by Mesozoic igneous rocks (lacking Late Paleozoic magmatic intrusives). This block is interpreted as belonging to the cratonic rocks located above the downgoing oceanic plate in the first stages of development of the associated subduction

channel (Urraza, 2014). This primitive regional contact that originally separated two well differentiated regions was further reactivated during the Andean Cycle (Urraza, 2014). The WNW-ESE ductile regional lineaments system shows evidence for sinistral shear component in plain view (Urraza, 2014). The regional trend and shear zones kinematics agree with those proposed for the almost parallel trending Lanahue regional fault zone defined by Glodny *et al.* (2008) in Chilean territory, in the northwestern extension of the study area.

The metamorphic rock sequence forming the southern domain of the AIMC can be correlated with part of the outcrops belonging to the Coastal Cordillera of south-central Chile (Fig. 13), considered to be part of an accretionary prism of Late Paleozoic to Mesozoic age (Glodny *et al.*, 2005, among others). The exposures of metamorphic rocks of center-west Argentina are smaller than those observed in Chile, partly due to the fact that abundant Andean plutonism and volcanism that largely obscures other possible records of rocks forming the accretionary prism.

The Coastal Cordillera metamorphic complex forms a coherent, trench-parallel belt exposed along the Pacific coast from 24°S to beyond 50°S. These metamorphic rocks were traditionally subdivided into two metamorphic complexes, the Western and Eastern Series (Fig. 13) that represent basal and frontal accretionary environments (Aguirre, 1972; Willner, 2005). The Western Series (WS) comprise intensively foliated metapsamopelitic rocks and metabasite intercalations with MORB and IOB (Ocean Island Basalts) signatures (Hyppolito *et al.*, 2014a, and references therein), whereas the Eastern Series (ES) lack metabasites and are represented by a less deformed very low-grade to high-grade metagreywacke-pelite sequence (Hyppolito *et al.*, 2015, and references therein; Willner, 2005).

TABLE 5. $^{40}\text{Ar}/^{39}\text{Ar}$ analytical data for incremental heating experiments on amphibole concentrates from Ñorquinco amphibolites

Hornblende

Laser Isotope Ratios											
Power(%)	$^{39}\text{Ar}/^{40}\text{Ar}$	2s	$^{36}\text{Ar}/^{40}\text{Ar}$	2s	r.i.	Ca/K	% ^{40}Ar atm	f ^{39}Ar	$^{40}\text{Ar}^*/^{39}\text{ArK}$	Age	2s
2.30	1646.41	53.43	5.09	0.19	0.004	0.28	91.35	4.79	142.458	622.04	± 224.26
2.70	190.40	11.83	0.47	0.03	0.002	0.14	73.11	7.78	51.197	248.88	± 43.12
3.00	74.42	4.39	0.12	0.01	0.008	0.02	46.78	9.33	39.608	195.46	± 24.88
3.50	55.03	2.02	0.04	0.00	0.041	0.04	18.93	54.92	44.611	218.72	± 15.68
4.00	48.54	2.06	0.03	0.00	0.018	0.07	15.66	14.13	40.942	201.69	± 17.76
5.50	55.94	3.20	0.03	0.00	0.005	0.02	18.14	9.05	45.794	224.17	± 24.74

J = 0.00288200 ± 0.00001441 Volume ^{39}ArK 0.007 x E-13 cm ³ NPT											
Integrated Date = 213.43 ± 9.52 Ma											
Plateau age = 212.7 ± 9.6 Ma (2s, including J-error of .5%) MSWD = 1.9, probability=0.10 Includes 95.2% of the ^{39}Ar steps 2 through 6											
Inverse isochron (correlation age) results, plateau steps: Model 1 Solution (±95%-conf.) on 6 points											
Age = 208.4 ± 9.9 Ma			Initial $^{40}\text{Ar}/^{36}\text{Ar}$ = 313 ± 11			MSWD = 1.5			Probability = 0.19		

Urraza (2014) proposed, for the first time, the correlation between the southern domain of the AIMC and the Chilean WS on the base of petrological, structural, geochemical, geochronological and paleogeographic similarities. In the present contribution, we propose that MORB-derived amphibolites intercalated in a Late Paleozoic metapelitic sequence in the AIMC, can be correlated with metabasite intercalations in meta-turbidites of the W-NW prolongation of the area of the present study (Glodny *et al.*, 2008, and references therein). Remarkable differences between the Ñorquino and Chilean territory metabasites are the lower pressures and greater metamorphic grade shown by the former and their adjacent rocks, compared to the latter and their enclosing rocks. Higher temperatures shown by Ñorquino amphibolites and their adjacent rocks can be easily explained considering that they form the easternmost outcrop of the basal accretionary prism that is the area in which the magmatic arc associated with the subduction was better developed. The magmatic arc is represented by abundant basic to felsic igneous intrusives, which are the appropriate sources of heat supply to the temperature increase in the basement rocks. On the other hand, low to intermediate pressures shown by Ñorquino amphibolites indicate that they remained above the subduction channel, that is, they were never dragged to great depths. This hypothesis is supported by geothermobarometry and pseudosection analysis, which indicate a counter-clockwise trajectory in accordance with

those previously established for other basement rocks of the AIMC (Urraza *et al.*, 2009, 2013). Similar counter-clockwise paths were proposed by Willner *et al.* (2004b) and Hyppolito *et al.* (2014b) for metabasites assigned to the early stages of subduction in the Coastal Cordillera accretionary complex of south-central Chile. The divergent pressures between the trajectories proposed by these authors and our work can be explained considering that the former were dragged down to high pressures along the subduction channel and, as indicated above, we consider that the metabasites studied here remained on top of it. Along the Chilean Coastal Cordillera, further north of the studied area, Hyppolito *et al.* (2014a, b) also mentioned amphibolites with MORB signatures. These authors considered metabasites of Punta Sirena region as tectonic slices of oceanic crust emplaced in the early stages of subduction, into predominantly aluminous metasedimentary rocks forming the basal portion of the accretionary prism against the continental margin.

According to evidence discussed above, we consider that Ñorquino amphibolites and adjacent metapelitic rocks represent the easternmost extension of the Western Series into Argentina territory. The southern AIMC domain formed part of the basal portion of an accretionary prism which was active in Late Paleozoic to Late Triassic time, as also proposed by other authors in several regions of the Coastal Cordillera of Chile (among others, Glodny *et al.*, 2005, Hyppolito *et al.*, 2014a, b, 2015).

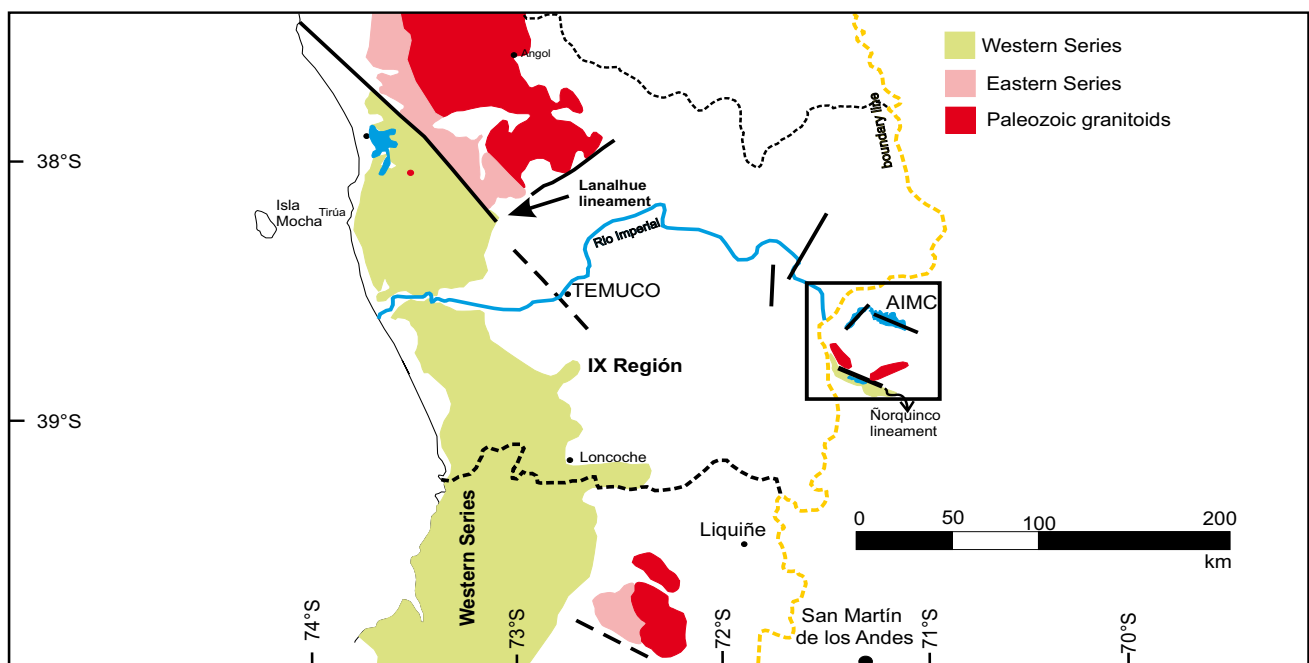


FIGURE 13. Sketch showing the proximity between pre- Andean exposures in Chile and the Paleozoic outcrops in AIMC as well as the main structural lineaments.

CONCLUSIONS

Structurally concordant lenses of mafic rocks intercalated in the metapelitic basement of the Ñorquinco lake area, southern sector of the AIMC, are defined on the basis of their geochemical signature as MORB-derived amphibolites.

Xenoliths of these MORB-derived amphibolites are also present in tonalites and granodiorites in the Ñorquinco lake sector. These metabasite inclusions affected the geochemical features of their host rocks, causing depletion in LREE and the disappearance of the slight Eu anomaly.

Considering variations in stable metamorphic assemblages and mineral compositions, two metamorphic events were recognized in the amphibolites intercalated in metapelites. M_1 was characterized by the mineral association Fe-MgAmp+Hbl_c+Pl+Bt+Qtz+Ilm+H₂O and developed at medium temperature-low pressure conditions. The overprinting M_2 event was characterized by the stable mineral association Hbl_r+Pl+Bt+Qtz+Ilm+H₂O, which implies an important increase in pressure and a slight increase in temperature. The baric peak of the trajectory represents onset of retrogression to lower P–T conditions after M_2 peak metamorphic conditions.

Conventional geothermobarometry combined with pseudosection analysis allow us to define a counterclockwise P–T path for the amphibolites of the Ñorquinco lake area. This trajectory is consistent with that of the surrounding metapelitic rocks and troctolites of the AIMC.

MORB-derived amphibolites of the AIMC are interpreted as fragments of oceanic crust emplaced in a sedimentary accretionary prism related to a NE-directed pre-Andean subduction zone. Early stages of subduction below the southwestern Gondwana margin during Late Paleozoic times promoted intense deformation of the accretionary prism and delamination of the oceanic slab and the consequent tectonic emplacement of mafic slices (precursors of amphibolites with MORB signatures) into the metasedimentary sequence. After that, both metapelitic and oceanic crust derived-mafic rocks record the same sequence of tectono-metamorphic events.

Petrological, geochemical, structural and geochronological data allow us to suggest that Ñorquinco rocks belong to the eastern extension of the Western Series of the Coastal Cordillera of Chile in central-west Argentina.

The ⁴⁰Ar/³⁹Ar cooling age of 212.7Ma is considered as the minimum age for the M_2 event registered in the amphibolites. This event is associated with a strong ductile deformation affecting the AIMC, which gave place to the

presently observed well defined mylonitic foliation. This age of metamorphism is consistent with the Late Triassic age proposed by various authors for the end of the accretionary prism activity in several localities of the Chilean territory.

ACKNOWLEDGMENTS

This contribution was funded by project PICT2008-N°1379, granted to Dra. Laura Grecco, and PUE Project 22920160100047CO, granted to INGEOSUR (CONICET-UNS). We thank Dr. Marcos Zentilli of Dahousie University, Dr. Mauricio González Guillot of Universidad Nacional de Tierra del Fuego, for their continuous support and Judy Schultz for the English corrections. We are grateful to Dr. Diaz Alvarado, Dr. Garcia Casco and Dr. Blanco Quintero for the constructive reviews.

REFERENCES

- Anderson, J.L., Smith, D.R., 1995. The effects of temperature and fO_2 on the Al-in-hornblende barometer. *American Mineralogist*, 80, 549-559.
- Aguirre, L., Hervé, E., Godoy, E., 1972. Distribution of metamorphic facies in Chilean outline. *Krystallinikum*, 9, 7-19.
- Boynnton, N.V., 1984. Cosmochemistry of the rare earth elements: meteorite studies. In: Henderson, P. (ed.). *Rare Earth Element Geochemistry. Development in Geochemistry II* Elsevier. 63-114.
- Casquet, C., Baldo, E., Pankhurst, R.J., Rapela, C.W., Galindo, C., Fanning, C.M., Saavedra, J., 2001. Involvement of the Argentine Precordillera Terrane in the Famatinian mobile belt: geochronological (U-Pb SHRIMP) and metamorphic evidence from the Sierra de Pie de Palo. *Geology*, 29, 703-706.
- Castro de Machuca, B., Perarnau, M., Alvarado, P., López, M.G., Sáez, M., 2012. A seismological and petrological crustal model for the southwest of the Sierra de Pie de Palo, San Juan (Argentina). *Revista de la Asociación Geológica Argentina*, 69, 177-184.
- Connolly, J.A.D., 1990. Multivariable phase diagrams; an algorithm based on generalized thermodynamics. *American Journal of Science*, 290, 666-718.
- Creixell, C., Ortiz, M., Arévalo, C., 2012. Geología del área Carrizalillo-El Tofo, regiones de Atacama y Coquimbo. Mapa escala 1:100.000. Santiago, Carta Geológica de Chile, n° 133-134, 82pp.
- Dale, J., Holland, T., Powell, R., 2000. Hornblende - garnet - plagioclase thermobarometry: a natural assemblage calibration of the thermodynamics of hornblende. *Contribution to Mineralogy and Petrology*, 140, 353-362.
- Dale, J., Powell, R., White, R., Elmer, F., Holland, J., 2005. A thermodynamic model for Ca–Na clinoamphiboles in Na₂O–CaO–FeO–MgO–Al₂O₃–SiO₂–H₂O–O for petrological calculations. *Journal of Metamorphic Geology*, 23, 771-791.
- Deer, W. A., Howie, R.A., Zussman, J., 1966. *An introduction to the rockforming minerals*. London, Longmans, Green and Co. Ltd, 528pp.

- Diener, J.F.A., Powell, R., White, R.W., Holland, T.J.B., 2007. A new thermodynamic model for clino and orthoamphiboles in the system $\text{Na}_2\text{O}-\text{CaO}-\text{FeO}-\text{MgO}-\text{Al}_2\text{O}_3-\text{SiO}_2-\text{H}_2\text{O}-\text{O}$. *Journal of Metamorphic Geology*, 25, 631-65.
- Duhart, P., McDonough, M., Muñoz, J., Martín, M., Villeneuve, M., 2001. El Complejo Metamórfico Bahía Mansa en la cordillera de la Costa del centro-sur de Chile ($39^{\circ}30'-42^{\circ}00'S$): geocronología K-Ar, $^{40}\text{Ar}/^{39}\text{Ar}$ y U-Pb e implicancias en la evolución del margen sur-occidental de Gondwana. *Revista geológica de Chile*, 28(2), 179-208.
- Ernst, W.G., Liou, J., 1998. Experimental phase equilibrium study of Al- and Ti-contents of calcic amphibole in MORB a semiquantitative thermometer. *American Mineralogist*, 83, 952-969.
- Fuentes, P., Díaz Alvarado, J., Rodríguez, N., Fernández, C., Breitzkreuz, C., Contreras A.A., 2018. Geochemistry, petrogenesis and tectonic significance of the volcanic rocks of the Las Tortolas Formation, Coastal Cordillera, northern Chile. *Journal of South American Earth Sciences*, 87, 66-86.
- García-Sansegundo, J., Farias, P., Gallastegui, G., Giacosa, R.E., Heredia, N., 2009. Structure and metamorphism of the Gondwana basement in the Bariloche region (North Patagonian Argentine Andes). *International Journal of Earth Sciences*, 98, 1599-1608.
- Gilbert, M.C., Helz, R.T., Poppand, R.K., Spear, F.S., 1982. Experimental studies of amphibole stability. In: Veblen, D.R., Ribbe, P.H. (eds.). *Amphiboles: petrology and experimental phase relations*. Washington, D.C, Mineralogical Society of America, pp 231-267.
- Glodny, J., Lohrmann, J., Echlter, H., Gräfe, K., Seifert, W., Collao, S., Figueroa, O., 2005. Internal dynamics of a paleoaccretionary wedge: insights from combined isotope tectonochronology and sandbox modelling of the South-Central Chilean forearc. *Earth and Planetary Science Letters*, 231, 23-39.
- Glodny, J., Echlter, H., Collao, S., Ardiles, M., Burón, P., Figueroa, O., 2008. Differential Late Paleozoic active margin evolution in South-Central Chile ($37^{\circ}\text{S}-40^{\circ}\text{S}$) the Lanalhue Fault Zone. *Journal of South American Earth Sciences*, 26, 397-411.
- Hawthorne, J.M., 1981. Stress relaxation behavior of biaxially oriented poly (ethylene terephthalate). *Journal of Applied Polymer Science*, 26(10), 3317-3324.
- Heredia, N., García-Sansegundo, J., Gallastegui, G., Farias, P.E., Giacosa, R., Hogn, E., Tubia, J., Luis Alonso, J., Busquets, P., Charrier, R., Clariana, P., Colombo, E., Cuesta, A., Gallastegui, J., Giambiagi, L., González-Menéndez, L., Limarino, C., Martín-González, E., Pedreira, D., Cardo, R., 2018. Pre-Andean phases of construction of the Southern Andes basement in Neoproterozoic-Paleozoic times. In: Folguera, A., Contreras, E., Heredia, N., Encinas, A., Iannelli, S., Oliveros, V., Dávila, E., Collo, G., Giambiagi, L., Maksymowicz, A., Iglesia, P., Llanos, P., Turienzo, M., Naipauer, M., Orts, D., Litvak, V., Álvarez, O., Arriagada, C. (eds.). *The Evolution of the Argentinian-Chilean Andes*. Springer, 111-131. DOI: 10.1007/978-3-319-67774-3_5.
- Hervé, E., 1987. Late Paleozoic subduction and accretion in Southern Chile. *UNESCO*, 11(3), 183-188.
- Hervé, E., 1988. Late Palaeozoic subduction and accretion in Southern Chile. *UNESCO*, 11, 183-188.
- Hervé, E., Faundez, V., Calderón, M., Massonne, H.J., Willner, A.P., 2007. Metamorphic and plutonic basement complexes. In: Moreno, T., Gibbons, W. (eds.). *The Geology of Chile*. London, the Geological Society, 5-19.
- Hyppolito, T., Garcia-Casco, A., Juliani, C., Meira, V.T., Hall, C., 2014. Late Paleozoic onset of subduction and exhumation at the western margin of Gondwana (Chilena Terrane): counterclockwise P-T paths and timing of metamorphism of deep-seated garnet-mica schist and amphibolite of Punta Sirena, Coastal Accretionary Complex. *Lithos*, 216-217, 409-434.
- Hyppolito, T., Juliani, C., Garcia-Casco, A., Meira, V., Bustamante, A., Hall, C., 2015. LP/HT metamorphism as a temporal marker of change of deformation style within the Late Paleozoic accretionary wedge of central Chile. *Journal of Metamorphic Geology*, 33, 1003-1024.
- Hyppolito, T., Angiboust, S., Juliani, C., Glodny, J., Garcia-Casco, A., Calderon, M., Chopin, C., 2016. Eclogite-, amphibolite- and blueschist-facies rocks from Diego de Almagro Island (Patagonia): Episodic accretion and Cretaceous thermal evolution of the Chilean subduction interface. *Lithos*, 264, 422-440.
- Holland, T., Blundy, J., 1994. Non-ideal interactions in calcic amphiboles and their bearing on amphibole-plagioclase thermometry. *Contribution to Mineralogy and Petrology*, 116, 433-447.
- Holland, T., Powell, R., 1998. An internally consistent thermodynamic data set for phases of petrological interest. *Journal of Metamorphic Geology*, 16(3), 309-343.
- Johnson, M.C., Rutherford, M.J., 1989. Experimental calibration of the aluminium-in-hornblende geobarometer with application to Long Valley caldera (California). *Geology*, 17, 837-841.
- Kato, T.T., 1985. Pre-Andean orogenesis in the Coast Ranges of central Chile. *Geological Society of America Bulletin*, 96, 918-924.
- Kato, T.T., Sharp, W., Godoy, E., 2008. Inception of a Devonian subduction zone along the southwestern Gondwana margin: $^{40}\text{Ar}/^{39}\text{Ar}$ dating of eclogite-amphibolite assemblage in blueschist boulders from the Coastal Range of Chile (41°S). *Canadian Journal of Earth Sciences*, 45, 337-351.
- Kato, T.T., Sharp, W.D., Godoy, E., 2009. Devonian-Carboniferous retro-eclogite (blueschist) boulders from the Cordillera de la Costa accretionary complex (41°S), Chile: Tectonic similarities to high grade blueschists of the California Coast Ranges. USA, Santiago, XII Congreso Geológico Chileno, 22-26.
- Koppers, A.P., 2002. Ar/Ar CALC – software for $^{40}\text{Ar}/^{39}\text{Ar}$ age calculations. *Computers and Geosciences*, 28, 605-619.
- Leake, B.E., 1964. The Chemical Distinction Between Ortho- and Para-amphibolites. *Journal of Petrology*, 5(2), 238-254.
- Leake, B.E., Wooley, A.R., Arps, C.E.S., Birch, W.D.S., Birch, W.D., Gilbert, M.C., Grice, J.D., Hawthorne, F.C., Kato, A., Kisch, H.J., Krivichev, V.G., Linthout, K., Laird, J., Mandarino, J.A.,

- Maresch, W.V., Nickel, E.H., Tock, N.M.S., Schumacher, J.C., Smith, D.C., Stephenson, N.C.N., Ungaretti, L., Whittaker, E., Youzhi, G., 1997. Nomenclature of amphiboles: report of the subcommittee on amphiboles of International Mineralogical Association, Commission on New Minerals and Mineral Names. *European Journal of Mineralogy*, 9, 623-651.
- Ludwig, K.R., 2003. Isoplot 3.09. A Geochronological Toolkit for Microsoft Excel. Berkeley Geochronology Center, 4 (Special Publication), 70pp.
- Martin, M., Kato, T., Rodríguez, C., Godoy, E., Duhart, P., McDonough, M., Campos, A., 1999. Evolution of Late Paleozoic accretionary complex and overlying forearc-magmatic arc south-central Chile (38-41°S): constraints for the tectonic setting along the southwestern margin of Gondwana. *Tectonics*, 12(4), 582-605.
- Martinez, J.C., Dristas, J.A., Massonne, H.J., 2011. Palaeozoic accretion of the microcontinent Chileña, North Patagonian Andes: high-pressure metamorphism and subsequent thermal relaxation. *International Geology Review*, 1, 1-19.
- Martínez Dopico, C.I., 2008. Metamorphic P-T constraints for the low-temperature assemblages overimposed on metamorphic and igneous rocks nearby Ñorquinco Lake, Aluminé, North-Patagonian Andes. Nice, 7th International Symposium on Andean Geodynamics, 319-321.
- Massonne, H.J., Calderón, M., 2008. P-T evolution of metapelites from the Guarguaráz Complex, Argentina: evidence for Devonian crustal thickening close to the western Gondwana margin. *Revista Geológica de Chile*, 35(2), 215-231.
- Massonne, H.J., Willner, A.P., 2008. Phase relations and dehydration behavior of psammopelite and mid-ocean ridge basalt at very-low-grade to low-grade metamorphic conditions. *European Journal of Mineralogy*, 20, 867-879.
- McDougall, I., Harrison, T.M., 1999. *Geochronology and Thermochronology by the $^{40}\text{Ar}/^{39}\text{Ar}$ method*. New York, Oxford University Press, 212pp.
- Meschede, M., 1986. A method of discriminating between different types of mid-ocean ridge basalts and continental tholeiites with the Nb-Zr-Y diagram. *Chemical Geology*, 56, 207-218.
- Misra, S.N., 1971. Chemical distinction of high-grade ortho and para-metabasites. *Norsk Geologisk Tidsskr.*, 51, 311-316.
- Newton, R.C., Haselton, H.T., 1981. Thermodynamics of the garnet-plagioclase- Al_2SiO_5 -quartz geobarometer. In: Newton, R.C., Navrotsky, A., Wood, B.J. (eds.). *Advances in physical geochemistry*. New York, Springer-Verlag, 1, 131-147.
- Otten, M.T., 1984. The origin of brown hornblende in the Artfjället gabbro and dolerites. *Contribution to Mineralogy and Petrology*, 86, 189-99.
- Pankhurst, R.J., Rapela, C.W., 1998. The proto-Andean margin of Gondwana: an introduction. In: Pankhurst, R.J., Rapela, C.W. (eds.). *The proto-Andean margin of Gondwana*. London, Geological Society, 142 (Special Publications), 1-9.
- Pankhurst, R.J., Rapela, C.W., Loske, W.P., Márquez, M., Fanning, C.M., 2003. Chronological study of the pre-Permian basement rocks of southern Patagonia. *Journal of South American Earth Sciences*, 16, 27-44.
- Pearce, J.A., 1983. Role of sub-continental lithosphere in magma genesis at active continental margins. In: Hawkesworth, C.J., Norry, M.J. (eds). *Continental Basalts and Mantle Xenoliths*, Cheshire, Shiva Publications, 203-249.
- Pearce, J.A., Cann, J.R., 1973. Tectonic setting of basic volcanic rocks determined using trace element analyses. *Earth Planetary Science Letter*, 19, 290-300.
- Raase, P., 1974. Al and Ti contents of hornblende, indicators of pressure and temperature of regional metamorphism. *Contributions to Mineralogy and Petrology*, 45, 231-236.
- Ramos, V.A., 1978. Estructura. *Relatorio Geología y Recursos Naturales del Neuquén*, 99-118.
- Ramos, V.A., 1984. Patagonia: un continente paleozoico a la deriva? IX Congreso Geológico Argentino, 2 (Actas), 311-325.
- Ramos, V.A., 1986. Tectonostratigraphy, as applied to analysis of South African Phanerozoic Basins by H. de la R. Winter, discussion. *Transactions Geological Society South Africa*, 87(2), 169-179.
- Ramos, V.A., 2000. Evolución tectónica de la Argentina. In: Caminos R. (ed.). *Argentina, Instituto de Geología y recursos minerales*, 29, 715-784.
- Ramos, V.A., 2004. Cuyania, an Exotic Block to Gondwana: Review of a Historical Success and the Present Problems. *Gondwana Research*, 7(4), 1009-1026.
- Rapela, C.W., 2000. The Sierras Pampeanas of Argentina: Paleozoic Building of the Southern Proto-Andes. In: Cordani U.G., Milani E.J., Thomaz-Filho A., Campos D.A. (eds.). *Tectonic Evolution of South America*. 31st International Geological Congress, Río de Janeiro, 381-387..
- Robinson, A.P., Spear, F.S., Schumacher, J.C., Laird, J., Klein, C., Evans, B.W., Doolan, B.L., 1982. Phase relations of metamorphic amphiboles: natural occurrence and theory. In: Veblen, D.R., Ribble, P.H. (eds.). *Amphiboles: Petrology and Experimental Phase Relations*. Mineralogical Society of America, *Reviews in Mineralogy*, 9B, 1-227.
- Shaw, D.M., Kudo, A.M., 1965. A test of discriminant function in amphibolite problem. *Mineralogical Magazine*, 34, 423-435.
- Spear, F.S., 1993. *Metamorphic Phase Equilibria and Pressure-Temperature-Time Paths*. Washington, Mineralogical Society of America, 799pp.
- Urraza, I.A., Grecco, L.E., Delpino, S.H., Arrese, M.L., 2006. Petrografía y estructura del sector norte del batolito de Aluminé, Neuquén, Argentina. San Luis (Argentina), 13° Reunión de Tectónica, Resúmenes, 61-62.
- Urraza, I., Grecco, L., Delpino, S., Zentilli, M., 2008a. Magmatic and tectonic evolution of the Aluminé belt, Patagonian Batholith, Neuquen, Argentina. Québec (Canada), 2008 GAC-MAC-SEG-SGA Annual Meeting, May 26-28 2008, Session: GS4 - Igneous Petrology, Volcanology and Metamorphic Petrology, Abstracts, 174.
- Urraza, I.A., Grecco, L.E., Delpino, S.H., Arrese, M.L., 2008b. Determination of rock ages by chemical analyses of Th, U,

- Pb in the mineral monazite (Ce, La, Th REE, U) PO4 using EPMA. Halifax, Nova Scotia, Canada, Annual General Meeting and Research Day, Institute for Research in Materials, Abstract, 36.
- Urraza, I., Delpino, S., Grecco, L., Arrese, M., 2009. Petrografía, geotermobarometría y geocronología del basamento del sector norte del Batolito Patagónico, Neuquén, Argentina. Río Cuarto, Argentina, Reunión de Tectónica, 14, Resúmenes, 34.
- Urraza, I.A., Grecco, L.E., Delpino, S.H., Arrese, M.L., Rapela, C.W., 2011. Petrología y Estructura del Complejo Ígneo-Metamórfico Aluminé, Provincia del Neuquén, Argentina. *Andean Geology*, 38(1), 98-117.
- Urraza, I.A., Delpino, S.H., Grecco, L.E., 2013. Presencia de Anfibolitas derivadas de MORB en el Basamento del Complejo Ígneo-Metamórfico Aluminé, Neuquén, Argentina. San Luis (Argentina), Simposio de Petrología Ígnea y Metalogénesis Asociada, Actas en Congreso, 95.
- Urraza, I.A., 2014. Evolución magmática y tectonometamórfica del Complejo Ígneo- metamórfico Aluminé, Provincia de Neuquén, Argentina. Doctoral Thesis. Bahía Blanca (Argentina), Universidad Nacional del Sur, 206pp.
- Urraza, I.A., Delpino, S.H., Grecco, L.E., 2015. Counterclockwise post-emplacement evolution of metatroctolites from Aluminé Igneous-Metamorphic Complex, Neuquén, Argentina. *Andean Geology*, 42(1), 36-55.
- Vaughan, A.P.M., Pankhurst, R.J., 2008. Tectonic overview of the West Gondwana margin. *Gondwana Research*, 13, 150-162.
- Whitney, D.L., Evans, B.W. 2010. Abbreviations for names of rock-forming minerals. *American Mineralogist*, 95, 185-187.
- Willner, A.P., Hervé, E., Thomson, S.N., Massonne, H.-J., 2004a. Converging PT-paths of Mesozoic HP-LT metamorphic units (Diego de Almagro Island, Southern Chile, 51°30'S): Evidence for juxtaposition during late shortening of an active continental margin. *Mineralogy and Petrology*, 81, 43-84.
- Willner, A.P., Glodny, J., Gerya, T.V., Godoy, E., Massonne, H., 2004b. A counterclockwise PTt path of high-pressure/low-temperature rocks from the Coastal Cordillera accretionary complex of south-central Chile: constraints for the earliest stage of subduction mass flow. *Lithos*, 75, 283-310.
- Willner, A. 2005. Pressure–Temperature Evolution of a Late Palaeozoic Paired Metamorphic Belt in North–Central Chile (34°–35°30'S). *Journal of Petrology*, 46(9), 1805-1833.
- Willner, A.P., Thomson, S.N., Kröner, A., Wartho, J.A., Wijbrans, J., Hervé, E., 2005. Time markers for the evolution and exhumation history of a late Paleozoic paired metamorphic belt in central Chile (34°–35°30'S). *Journal of Petrology*, 46, 1835-1858.
- Willner, A.P., Gerdes, A., Massonne, H.J., 2008. History of crustal growth and recycling at the Pacific convergent margin of South America at latitudes 29-36°S revealed by a U-Pb and Lu-Hf isotope study of detrital zircon from late Paleozoic accretionary systems. *Chemical Geology*, 253, 114-129.
- Willner, A.P., Massone, H.J., Ring, U., Sudo, M., Thomson, S.N., 2011. P–T evolution and timing of a late Paleozoic fore-arc system and its heterogeneous Mesozoic overprint in north-central Chile (latitudes 31–32°S). *Geological Magazine*, 149, 177-207.

**Manuscript received February 2019;
revision accepted November 2019;
published Online November 2019.**